Probing the bioavailability of dissolved iron to marine eukaryotic phytoplankton using *in situ* single cell iron quotas

Yeala Shaked[*1,2], Benjamin S. Twining[*3], Alessandro Tagliabue[4], and Maria. T. Maldonado[5]

[1] Freddy and Nadine Herrmann Institute of Earth Sciences, Hebrew University, Jerusalem, 91904, Israel.

[2] Interuniversity Institute for Marine Sciences, Eilat, 88103, Israel.

[3] Bigelow Laboratory for Ocean Sciences, 60 Bigelow Dr., East Boothbay, Maine 04544 USA.

[4] School of Environmental Sciences, University of Liverpool, Liverpool, L69 3GP, United Kingdom.

[5] Department of Earth, Ocean and Atmospheric Sciences, University of British Columbia, Vancouver, V6T 1Z4, Canada.

Corresponding authors: Yeala Shaked (yeala.shaked@mail.huji.ac.il) and Ben Twining (btwining@bigelow.org)

Key Points:

- A proxy for dissolved Fe (dFe) bioavailability in low-Fe oceanic regions is established using individual phytoplankton Fe content, dFe concentrations, and modeled growth rates.
- Grand average dFe bioavailability is extracted for low-Fe regions, as values are nearly constant across varying temperature, dFe concentrations, and phytoplankton taxa.
- The bioavailability proxy indicates dFe is highly available in these low-Fe systems and can further be used to calculate *in situ* Fe uptake rates and biological Fe residence times and for validating global model output.

Abstract

We present a new approach for quantifying the bioavailability of dissolved iron (dFe) to oceanic phytoplankton. Bioavailability is defined using an uptake rate constant ($k_{in\text{-}app}$) computed by combining data on: i) Fe content of individual *in situ* phytoplankton cells; ii) concurrently-determined seawater dFe concentrations; and iii) growth rates estimated from the PISCES model. We examined 930 phytoplankton cells, collected between 2002-2016 from 45 surface stations during 11 research cruises. This approach is only valid for cells that have upregulated their high-affinity Fe uptake system, so data was screened, yielding 560 single cell $k_{in\text{-}app}$ values from 31 low-Fe stations. We normalized $k_{in\text{-}app}$ to cell surface area (S.A.) to account for cell-size differences.

The resulting bioavailability proxy ($k_{in\text{-}app}$/S.A.) varies among cells, but all values are within bioavailability limits predicted from defined Fe complexes. *In situ* dFe bioavailability is higher than model Fe-siderophore complexes and often approaches that of highly-available inorganic Fe′. Station averaged $k_{in\text{-}app}$/S.A. are also variable but show no systematic changes across location, temperature, dFe, and phytoplankton taxa. Given the relative consistency of $k_{in\text{-}app}$/S.A. among stations (ca. 5-fold variation), we computed a grand-averaged dFe availability, which upon normalization to cell carbon (C) yields $k_{in\text{-}app}$/C of 42,200 ± 11,000 L mol C^{-1} d^{-1}. We utilize $k_{in\text{-}app}$/C to calculate dFe uptake rates and residence times in low Fe oceanic regions. Finally, we demonstrate the applicability of $k_{in\text{-}app}$/C for constraining Fe uptake rates in earth system models, such as those predicting climate mediated changes in net primary production in the Fe-limited Equatorial Pacific.

Plain Language Summary

In many oceanic regions, iron exerts strong control on phytoplankton growth, ecosystem structure and carbon cycling. Yet, iron bioavailability and uptake rates by phytoplankton in the ocean are poorly constrained. Recently, Shaked et al. (2020) established a new approach for quantifying the availability of dissolved Fe (dFe) in natural seawater based on its uptake kinetics by Fe-limited cultured phytoplankton. Here, we extend this approach to *in situ* phytoplankton, establishing a standardized proxy for dFe bioavailability in low-Fe oceanic regions.

Bioavailability is estimated through single cell Fe uptake constants, calculated by combining measured Fe contents of individual phytoplankton cells collected from multiple regions with concurrently-measured dFe concentrations, as well as modeled growth rates. We then utilize this proxy for: a) comparing dFe bioavailability among organisms and regions; b) calculating dFe uptake rates and residence times in low-Fe oceanic regions; and c) constraining Fe uptake parameters of earth system models to better predict ocean productivity in response to climate-change.

1. Introduction

Marine phytoplankton generate about half of Earth's oxygen and play important roles in ocean carbon uptake and cycling (Sigman & Hain, 2012). Phytoplankton photosynthesis is often limited by the supply of macro and micro nutrients (Saito et al., 2008; Moore et al., 2013). In particular, the micronutrient iron (Fe), present at sub-nanomolar concentrations in most of the upper waters (Johnson et al., 1997), exerts strong control on phytoplankton biomass and production rates, as well as microbial community structure, trophic dynamics and elemental cycling in both the coastal and open ocean (Tagliabue et al., 2017). Significant research efforts to understand, constrain, and accurately model the biogeochemical Fe cycling are underway, given its importance to ocean productivity and the global carbon cycle (Boyd and Ellwood, 2010; Tagliabue et al., 2016).

Over the past four decades algal physiologists have examined how cultured marine phytoplankton cope with Fe limitation and acquire Fe from their external milieu (reviewed by Shaked & Lis, 2012; Marchetti & Maldonado, 2016; Sutak et al., 2020). Recent phytoplankton genomic studies have expanded our understanding of Fe homeostasis and uptake, documenting multiple Fe transport pathways (e.g. Allen et al., 2008; Groussman et al., 2015; Kustka et al., 2007; Lommer et al., 2007; Morrissey & Bowler, 2012; McQuaid et al., 2018). Meanwhile, sea-going oceanographers have investigated Fe uptake and cycling by *in situ* plankton communities (e.g. Bowie et al., 2001; Cabanes et al., 2020; Maldonado & Price, 1999). These studies have been complemented by global-scale surveys of Fe concentrations and speciation via the international GEOTRACES program (Anderson, 2020; Mawji et al., 2014; Schlitzer et al., 2018), as well as by efforts to determine the molecular speciation of dFe (e.g. Boiteau et al., 2016, 2018; Macrellis et al., 2001; Mawji et al., 2008). Together, these studies have greatly expanded our understanding of dFe concentration and speciation, as well as sources, and sinks in the upper ocean.

Yet, there remains considerable uncertainty about the connection between dFe speciation and dFe bioavailability to resident phytoplankton. Dissolved Fe speciation in the upper ocean is largely dominated by a heterogenous pool of organic complexes, mostly molecularly uncharacterized but with distinct chemical reactivities (e.g. Gledhill & van den Berg, 1995; Rue & Bruland, 1995; Bundy et al., 2014, 2018; Fitzsimmons et al., 2015) and undefined bioavailability (e.g. Worms et al., 2006; Hassler et al., 2012; Shaked & Lis, 2012). Furthermore, even if it was possible to link dFe speciation to bioavailability in natural seawater, the speciation of dFe in the surface ocean is highly dynamic, with ligand-exchange, photochemical, and biologically-mediated reactions that drive rapid interconversion among dFe species (e.g. Barbeau et al., 2001; Waite, 2001; Shaked, 2008). Additionally, resident phytoplankton actively alter their physiology and transport mechanisms to access and internalize different Fe substrates (e.g. Marchetti et al., 2012), further complicating efforts to constrain the bioavailability of individual chemical Fe species. Considering the dynamics in Fe speciation, it has been suggested that total dFe is the most appropriate indicator of bioavailable Fe in the ocean (Bruland et al., 2001), although others have proposed that labile particulate species might also be important on timescales relevant to biological productivity (Hurst et al., 2010). Most numerical models of ocean biogeochemistry currently assume that all Fe species in the dissolved phase are equally bioavailable, and thus use dFe concentrations in seawater to estimate biological Fe uptake (Tagliabue et al., 2016).

Seeking a simplified and generalized definition and quantification method for Fe bioavailability in the ocean, Shaked et al. (2020) presented a standardized proxy that relies on the uptake kinetics of Fe-limited phytoplankton. The bioavailability of natural dFe was probed through short-term

uptake experiments with low-level radiotracer using several cultured Fe-limited phytoplankton species belonging to the major taxa occurring in the ocean. All tested phytoplankton species were found to acquire natural dFe, including organic complexes, at comparable rates when accounting for their surface area (S.A.). Normalizing these uptake rates to cell S.A. and dFe concentration in the water sample, Shaked et al. (2020) established the bioavailability proxy - $k_{in\text{-}app}$/S.A. Testing 12 seawater types from different basins and depths, they observed relatively small differences between water types and reported a grand average value for dFe availability in natural seawater.

Here, utilizing *in situ* phytoplankton and dFe data from the ocean, we extend this approach and evaluate dFe bioavailability across different Fe-limited ocean regions. We first calculated *in situ* steady-state Fe uptake rates of diverse natural phytoplankton communities by combining single cell Fe content (i.e., quotas) measured with synchrotron X-ray fluorescence with growth rates estimated from a biogeochemical model. Then, utilizing measured, ambient dFe concentrations, we calculated single-cell Fe uptake rate constants ($k_{in\text{-}app}$), which upon normalization to cell S.A. ($k_{in\text{-}app}$/S.A.) or cell carbon ($k_{in\text{-}app}$/C), serve as a standardized proxy of dFe availability. We verify and establish this proxy for Fe-limited phytoplankton and report that dFe availability does not vary systematically with location, temperature, dFe concentrations or phytoplankton groups, enabling calculation of grand mean oceanic dFe bioavailability proxy for low Fe regions. We then utilize this proxy for: a) comparing dFe bioavailability among organisms and regions; b) calculating dFe uptake rates and residence times in low Fe oceanic regions; and c) constraining Fe uptake parameters of earth system models to better predict ocean productivity in response to climate-change.

2 Materials and Methods

2.1 Analytical approach

Following the framework of Lis et al. (2015b) and Shaked et al. (2020), we infer oceanic dFe availability from uptake rates calculated using single-cell Fe quotas determined with synchrotron X-ray fluorescence and growth rates estimated from a biogeochemical model (details below). We then divide calculated Fe uptake rates by measured ambient dFe concentrations to obtain an uptake rate constant – $k_{in\text{-}app}$ – as shown in equation 1:

Eq. 1: $k_{in\text{-}app}$ (L cell^{-1} d^{-1}) =
Fe quota (mol Fe cell^{-1}) x growth rate (d^{-1}) / SW dFe concentration (mol Fe L^{-1})

This approach is based on several assumptions, namely that dFe is the substrate for uptake by phytoplankton and that dFe concentrations remain relatively constant during the cell growth (i.e. cell Fe quota reflect ambient Fe concentrations). We then propose to apply $k_{in\text{-}app}$ as a standardized proxy of dFe bioavailability in low-Fe regions. The following conditions have to be met for $k_{in\text{-}app}$ to serve as a bioavailability proxy: 1) cells are Fe-limited or Fe-stressed, such that the high-affinity Fe uptake system is active; 2) $k_{in\text{-}app}$ remains relatively stable across varying degrees of Fe-stress; 3) $k_{in\text{-}app}$ is proportional to the surface area (S.A.) of the cell, allowing normalization to S.A.; and 4) $k_{in\text{-}app}$ remains relatively stable between cells from different taxonomic groups. We test and verify these assumptions and conditions in the results section. See SI section S1 for additional information.

2.2 Datasets and parameters

Our analysis draws upon published datasets available in data repositories (GEOTRACES intermediate data product, BCO-DMO) and scientific publications (see Fig. 1 legend for a full list). We analyzed 8 datasets collected during 11 cruises across 4 ocean basins between 2002 and 2016 (Fig. 1). Detailed analytical methods and data collection protocols can be found in the GEOTRACES cookbook (Cutter et al., 2017) and individual publications (Twining et al., 2003, 2005, 2011, 2015, 2019, 2021). Information on cell Fe quota and size measurements, which are key to our analysis, is detailed below. Some published dFe concentrations from SOFeX project (Twining et al., 2004) were found to be contaminated and hence were replaced with values provided by Z. Chase (personal communication), who analyzed the original samples.

Cellular Fe quota, cell dimensions and C quota

The Fe content of individual phytoplankton cells (i.e., the Fe quota), collected at 20 m depth, was measured by synchrotron X-ray fluorescence (SXRF). Detailed methods are provided elsewhere (Twining et al., 2003, 2005, 2011, 2015, 2019), and consistent methods and analytical standards have been applied throughout the studies. Carbon quotas for each cell were calculated from biovolume estimates from 2-3 cell dimensions from a light micrograph, after applying cell shape, volume, and surface area equations of Hillebrand et al. (1999). Calculated biovolumes were converted to cellular C using the relationships for diatoms and non-diatoms provided by Menden-Deuer & Lessard (2000). The mean number of cells analyzed in each station was 20 (ranged from 10-50, Table 1). Cells were broadly classified into three groups: diatoms, flagellates or picoeukaryotes. Some stations only contained one phytoplankton group, while others had two or three groups (Table 1).

Growth rate evaluation

For each station, growth rates were calculated based on sampling month using the PISCES-V2 model (Aumont et al., 2015). Modeled growth rates, affected by a combination of temperature, light and nutrient limitation, were calculated separately for two phytoplankton functional types: diatoms and nanophytoplankton. For simplicity, all cells other than diatoms (mostly defined as flagellates in the original SXRF analysis) were assigned growth rates of nanophytoplankton. The model-derived growth rates were available at a spatial resolution of 2 degrees in longitude and 2 x cos(latitude), with the resolution enhanced to 0.5 x 0.5 degree around the equator. The growth rate output of the PISCES-V2 model typically ranged from 0.2 to 0.8 d^{-1} for stations with varying degrees of Fe-limitation, and as low as 0.03 d^{-1} for N-limited stations (Table 1). The model growth rates compared well with the few available *in situ* growth rates reported for these cruises (Landry et al., 2011; Selph et al., 2011). Further details on the estimation of growth rates and its effect on our analysis is provided in the supplementary material (SI Section S2).

2.3 Dataset screening and selection criteria

We excluded cells collected from artificially Fe-fertilized stations (as during SOFeX; Twining et al., 2004), and cells collected from the deep-chlorophyll maximum that may have been light limited and thus have relatively high Fe quotas (Maldonado et al., 1999). We calculated $k_{in\text{-}app}$ for the remaining 930 cells collected from 45 unperturbed surface stations from 8 research campaigns

(including 11 cruises). Then we defined for each station whether cells are Fe-limited, Fe-replete or N-limited (Table 1, see criteria below).

Determination of Fe limitation

Only cells from Fe-limited populations were used to probe dFe availability, because under these sub-saturating dFe conditions the cells upregulate their high affinity Fe-uptake systems (Hudson & Morel, 1990; Maldonado & Price, 2001; Shaked et al., 2005), and their Fe uptake rates are directly proportional to *in-situ* dFe concentrations (for details see Shaked et al., 2020). Each data set was evaluated with regards to hydrography, temperature, nutrient (Fe, NO_3^-) concentrations, and, when available, physiological and molecular markers of Fe-limitation and grow-out experiments conducted in parallel. We evaluated the primary limiting nutrient for phytoplankton growth in each of the stations based on measured concentrations of dFe in nM and NO_3^- in µM and the ratio of these according to the criteria of Browning et al., (2017). Stations with [dFe] < 0.6 nM and $\log_{10}(N_{\mu M} / Fe_{nM}) > 1$, were defined as Fe-limited. Stations with $[NO_3^-] <1$ µM and $\log_{10}(N/Fe) < 1$, were defined as N-limited (regardless of [dFe]). Stations with [dFe] > 0.6 nM were defined as Fe-replete (regardless of $\log_{10}(N/Fe)$). A few stations with [dFe] < 0.6 nM and $\log_{10}$ (N/Fe) ranging between 0-1, were defined as co-limited by Fe and NO_3^- . Only stations defined as Fe-limited or co-limited by Fe and NO_3^- were included in the final analysis and used for probing oceanic dFe availability (Table 1). Even under low-Fe conditions, individual cells may accumulate excess Fe (Twining et al., 2021). Thus, the status of Fe-limitation by individual cells was further assessed by their cellular Fe quotas, which typically range between 1 and 50 µmol Fe/mol C (Marchetti & Maldonado, 2016). Cells demonstrating luxury Fe uptake, defined here as Fe:C > 100 µmol Fe/mol C, were excluded from dFe availability analysis (at most 5 cells per station in only few of the Fe-limited stations).

Steady state growth

The calculation of steady-state dFe uptake rates from cell Fe quotas and growth rates is valid only for steady state growth (Huntsman & Sunda, 1980b; Sunda et al., 2005), which was assumed to occur *a priori* in most stations. This steady-state condition was probably not met in some dynamic systems receiving episodic Fe supply, such as upwelling regions or dust impacted areas. Two stations over the Peru shelf were defined as non-steady state based on a mismatch between [dFe] and mean Fe quota (as compared with other data from the same cruise, (Twining et al., 2021) and were not included in the dFe bioavailability analysis (Table 1).

2.4 Statistical analysis

Data processing was conducted using R Studio, and statistical testing was conducted with JMP statistical software (v11, SAS). Data were $\log_{10}$-transformed to normalize data, which was confirmed with Shapiro-Wilk tests. Comparisons between cell types and between geographic locations were tested with Student t-tests and one-way ANOVAs. An analysis of co-variance model (ANCOVA) was used to test for statistically significant effects on $k_{in\text{-}app}$ by simultaneous variations of cell type, geographic location, and dFe (statistical analyses are shown in SI sections S3 and S4).

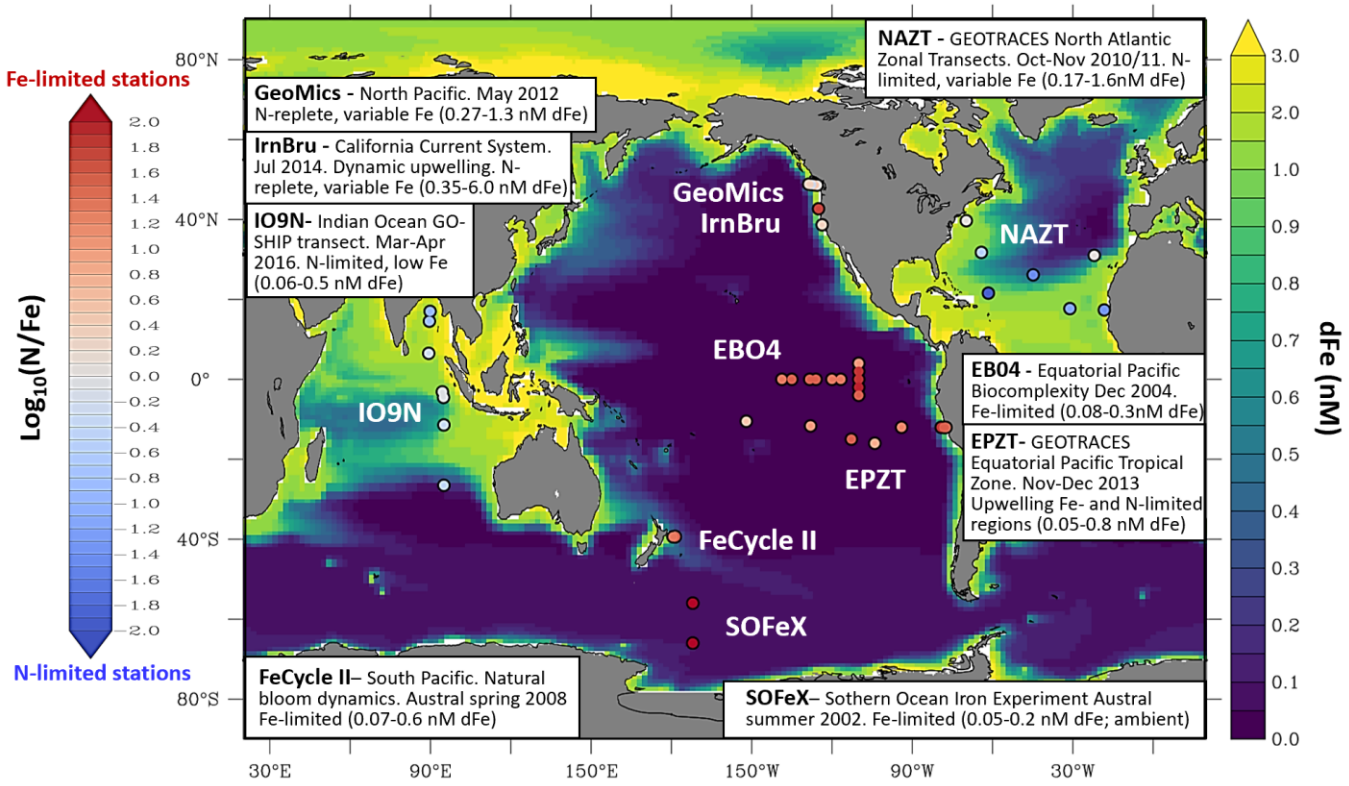

Figure 1. Dataset of single cell Fe quota collected from 2002-2016 during 8 research projects. Cruise stations plotted on a map of surface dFe concentrations estimated by PISCES model. Stations are colored according to the nutrient limitation index of Browning et al. (2017) using the observed nutrient concentrations. The dataset was screened and only Fe-limited stations were included in the assessment of dFe bioavailability. Cruise data used for our study was based on the following publications: (**SoFeX -** Coale et al., 2004; Twining et al. 2004a & 2004b); (**EB04 -** Brzezinski et al., 2011; Kaupp et al., 2011; Selph et al., 2011; Twining et al., 2011); (**FeCycle II** - Boyd et al., 2012; Ellwood et al., 2014; King et al., 2012; Wilhelm et al., 2013); (**NAZT-** Hatta et al., 2015; Sedwick wt al., 2015; Twining et al., 2015); (**GeoMics -** Chappell et al., 2019; Twining et al., 2021); (**IrnBru -** Boiteau et al., 2018; Cohen et al., 2018; Lampe et al., 2018; Mellett et al., 2018; Till et al., 2019); (**EPZT -** Boiteau et al., 2016; Moffett & German, 2018; Twining et al., 2021); (**IO9N -** Baer et al., 2019; Twining et al., 2019).

Table 1 Information on cruises and dFe bioavailability analysis. Stations were defined according to the primary limiting nutrient based on N and Fe concentrations and the $\log_{10}(N_{\mu M} / Fe_{nM})$ criteria of Browning et al. (2017), aided with published findings on these cruises. Stations not considered Fe-limited (marked in blue) were not included in the final assessment of dFe bioavailability (indicated as No in the Included columns).

Project	Station	Lat	Long	Temp	[dFe]	[NO_3]	log (N/Fe)	Degree of limitation		Cell types &	Cell #	Model growth rates (d^{-1})$		Average k_{in-app}/S.A.	SE	Included	Comments
		N	E	C	(nM)	(uM)		Fe	NO_3^-			Diatom	Flag			(Yes/No)	
SOFeX Southern Ocean	19	-66.0	-172.0	-0.7	0.14	29	2.3	++	--	Mixed	22	0.18	0.39	2.7E-10	1E-10	Yes	Fe-limited ambient water (no Fe-seeded stations)
	27	-66.0	-172.0	-0.6	0.14	28	2.3	++	--	Mixed	27	0.18	0.39	2.1E-10	9E-11	Yes	
	7	-56.0	-172.0	7.2	0.14	22	2.2	++	--	Flag	17	0.17	0.27	2.1E-10	5E-11	Yes	
	11	-56.0	-172.0	7.2	0.14	21	2.2	++	--	Flag	11	0.17	0.27	2.5E-10	9E-11	Yes	
FeCycle II South Pacific	U5715 & 5721	-39.3	-178.6	14	0.60	2.8	0.7	+	--	Diatom	14	0.35	0.48	3.1E-10	7E-11	Yes	Bloom initiation. Mildely Fe limited
	U5727	-39.4	-178.8	14	0.59	3.5	0.8	+	--	Mixed	38	0.35	0.48	1.7E-10	5E-11	Yes	
	U5731	-39.4	-178.7	14	0.12	3.4	1.4	++	--	Mixed	23	0.23	0.32	2.2E-10	3E-11	Yes	Bloom peak. Fe limited
	U5750	-39.4	-178.5	14	0.07	2.5	1.5	++	--	Mixed	22	0.23	0.32	2.5E-10	1E-10	Yes	Bloom decline.
	U5756 & 5776	-39.4	-179.4	14	0.13	3.0	1.4	++	--	Mixed	29	0.23	0.32	1.7E-10	3E-11	Yes	Strongly Fe limited
EBO4 Equatorial Pacific	2	4.0	-110.0	26	0.079	0.75	1.0	++	--	Flag	21	0.34	0.55	8.0E-10	2E-10	Yes	Fe-limited
	4	2.0	-110.0	25	0.079	6.3	1.9	++	--	Mixed	21	0.43	0.65	6.6E-10	8E-11	Yes	
	7	0.0	-110.0	24	0.079	6.2	1.9	++	--	Mixed	35	0.50	0.78	6.2E-10	1E-10	Yes	
	10	-2.0	-110.0	24	0.079	7.1	2.0	++	--	Mixed	15	0.47	0.73	1.3E-09	2E-10	Yes	
	12	-4.0	-110.0	25	0.20	8.0	1.5	+	--	Mixed	15	0.49	0.78	2.0E-10	3E-11	Yes	Mildly Fe limited (growth limitation for large diatoms)
	14	0.0	-116.7	25	0.24	7.4	1.4	+	--	Mixed	19	0.49	0.77	2.1E-10	3E-11	Yes	
	16	0.0	-120.0	25	0.15	3.5	1.4	+	--	Mixed	8	0.49	0.77	3.0E-10	9E-11	Yes	
	20	0.0	-126.0	25	0.24	7.5	1.5	+	--	Mixed	18	0.47	0.76	2.9E-10	7E-11	Yes	
	22	0.0	-128.3	26	0.20	6.6	1.5	+	--	Mixed	7	0.48	0.77	2.4E-10	1E-10	Yes	
	26	0.0	-135.0	26	0.16	6.1	1.6	+	--	Mixed	40	0.49	0.80	2.5E-10	3E-11	Yes	
	28	0.0	-138.7	26	0.32	5.8	1.3	+	--	Mixed	21	0.50	0.81	2.4E-10	1E-10	Yes	
EPZT Equatorial Pacific	1	-12.0	-79.2	18	0.11	7.5	1.8	+	--	Mixed	26	0.44	0.80	9.3E-10	2E-10	Yes	Mildly Fe limited
	3	-12.0	-77.7	15	0.82	19	1.4	--	--	Mixed	13	0.57	1.2	3.8E-10	2E-10	No	Non S.S-high dFe low Q
	4	-12.0	-77.8	16	0.41	12	1.5	?	--	Mixed	23	0.57	1.2	1.4E-09	3E-10	No	Non S.S-high Q low dFe
	5	-12.0	-78.2	17	0.27	12	1.6	+	--	Mixed	12	0.57	1.2	5.5E-10	2E-10	Yes	Mildly Fe limited
	11	-12.0	-94.0	21	0.049	0.85	1.2	++	--	Mixed	16	0.32	0.53	1.0E-09	2E-10	Yes	Stongly Fe limited
	15	-16.0	-104.0	22	0.078	0.57	0.9	++	--	Mixed	17	0.12	0.20	3.5E-10	1E-10	Yes	
	18	-15.0	-112.8	24	0.087	3.8	1.6	+	?	Mixed	13	0.14	0.23	2.4E-10	4E-11	Yes	Fe-limited
	26	-11.7	-128.0	27	0.17	2.3	1.1	+	?	Mixed	16	0.18	0.29	1.9E-10	1E-10	Yes	
	36	-10.5	-152.0	29	0.082	0.32	0.6	+	+	Mixed	29	0.082	0.18	1.5E-10	2E-11	Yes	N-Fe co-limited
GeoMICS North Pacific	P8	48.8	-128.7	11	0.27	0.35	0.1	+	-	Diatom	18	0.28		4.7E-10	1E-10	Yes	Mildly Fe limited
	P6	48.7	-127.7	11	0.46	2.0	0.6	?	-	Diatom	13	0.17		4.8E-11	1E-11	No	Not Fe limited
	P4	48.7	-126.7	11	0.64	0.37	-0.2	--	-	Diatom	27	0.17		8.4E-11	2E-11	No	
	P1	48.6	-125.5	9.0	1.3	3.1	0.4	--	-	Diatom	27	0.28		6.7E-11	3E-11	No	
IrnBru California Current	28	42.7	-125.0	11	0.35	17	1.7	+	--	Diatom	14	0.37		3.3E-10	3E-11	Yes	Mildly Fe limited
	2	38.7	-123.7	11	5.7	14	0.4	--	--	Diatom	12	0.43		1.2E-10	4E-11	No	Not Fe limited
IO9N Indian Ocean	87	-26.5	95	24.3	0.12	< 0.05	-0.4	+	++	Flag	20		0.030	1.2E-11	3E-12	No	N limits growth, low Fe
	127	-4.53	94.87	30.2	0.06	< 0.05	-0.1	+	++	Flag	16		0.059	4.8E-11	1E-11	No	
	130	-3.13	94.43	30.7	0.07	< 0.05	-0.1	+	++	Flag	18		0.067	3.3E-11	8E-12	No	
	189	14.5	89.59	30.2	0.38	< 0.05	-0.9	+	++	Flag	19		0.65	9.1E-11	2E-11	No	
	194	17	89.85	29.4	0.49	< 0.05	-1.0	+	++	Flag	11		2.5	2.0E-10	7E-11	No	
NAZT North Atlantic	2010-5	31.0	-22.0	24	0.18	0.20	-0.6	?	++	Flag	14		0.026	3.4E-11	2E-11	No	N limits growth, high Fe
	2010-9	17.4	-18.3	28	0.88	0.035	-1.2	--	++	Flag	19		0.16	4.3E-11	9E-12	No	
	2010-99	17.7	-31.1	27	0.42	0.026	-0.9	--	++	Mixed	16	0.01	0.031	1.7E-11	4E-12	No	
	2010-153	21.6	-61.6	28	1.6	0.020	-1.5	--	++	Flag	10		0.032	5.4E-12	2E-12	No	
	2011-1	39.7	-69.8	19	0.62	0.57	-1.1	--	?	Mixed	10	0.26	0.35	3.3E-10	8E-11	No	

All samples are from mixed layer

&- Cell types - Mixed ref to all cell types, including diatoms, flaggelates (=Flag) and pico-eukaryptes.

$- Model output growth rates were for two phytoplankton groups, Diatoms and Nanoflaggelates (titled here Flag)

3. Results

3.1 Choice of dFe (over Fe') as a probe of iron bioavailability in the ocean

Following Shaked et al. (2020) we consider dFe – the entire pool of dissolved Fe complexes – as the substrate for uptake by naturally-occurring Fe-limited phytoplankton when calculating $k_{in\text{-}app}$ (SI Table S1). The choice of dFe rather than Fe' – the sum of inorganic Fe species – may appear to conflict with culture studies that report Fe' as the substrate for uptake (Shaked et al., 2005; Sunda & Huntsman, 1995). However, most culture work has been conducted in media buffered by a large excess of EDTA, in which EDTA complexation intentionally dominates Fe speciation, and the Fe' concentrations are largely in the pM range (Shaked & Lis, 2012; Sunda et al., 2005). While Fe' is undoubtedly an important substrate for phytoplankton uptake in the ocean (Morel et al., 2008), ocean Fe' concentrations calculated from electrochemical Fe speciation measurements fail to account for the rapid *in situ* cycling of Fe' (Gledhill & Buck, 2012). Indeed, *in situ* Fe uptake studies demonstrate that the supply rates of Fe' in surface waters is too slow to account for the rates of Fe uptake, indicating that ocean phytoplankton access organically-bound dFe species (Maldonado & Price, 1999; Hassler et al., 2011; King et al., 2012; Maldonado et al., 2005; Mellett et al., 2018).

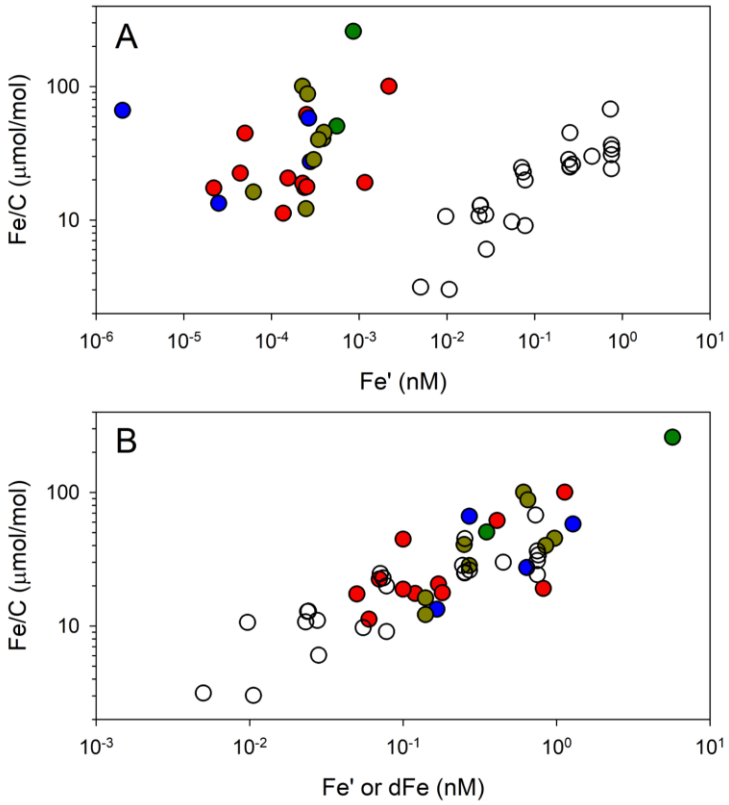

Fig 2. Comparison of iron quotas measured in ocean phytoplankton (colored symbols) or laboratory cultures (white symbols) as a function of Fe concentration. Quotas are plotted either against (A) Fe', as calculated either for EDTA-buffered media or for natural seawater, or (B) calculated Fe' for laboratory data and measured dFe for ocean samples. Ocean phytoplankton were collected from the South Pacific (red), North Pacific (blue), coastal California current (green), and the North Atlantic (brown). Data are from (Buck et al., 2015, 2018; Chappell et al., 2019; Mellett et al., 2018; Twining et al., 2015, 2021). Laboratory phytoplankton data are from (Sunda & Huntsman, 1995). Note that in A oceanic Fe' is calculated from speciation measurements that do not account for short term photochemically produced Fe'.

A comparison of Fe quotas measured in natural phytoplankton populations and laboratory cultures shows 1000-fold divergence when plotted against concurrently-evaluated Fe' (Fig. 2a). However, when Fe quotas of natural phytoplankton are plotted rather as a function of measured dFe they closely agree with those of the cultures grown in EDTA-buffered media (Fig. 2b). This supports our use of dFe as the bioavailable Fe pool in natural systems, following the approach of Shaked et al. (2020).

3.2 Proportionality between $k_{in\text{-}app}$ and surface area (S.A.) of individual cells

Previous studies have demonstrated proportionality between Fe uptake rates and S.A. in Fe-limited cells, reflecting physiological maximum density of high-affinity transport proteins at the cell surface (Hudson & Morel, 1990; Lis et al., 2015; Maldonado & Price, 2001; Morel, 2008; Shaked & Lis, 2012; Sunda & Huntsman, 1997; Sunda et al., 2005). Graphically, such proportionality should yield a slope of unity (1) on a log-log plot of $k_{in\text{-}app}$ versus S.A, with a high linear correlation coefficient (R^2). Indeed, slopes nearing one and high correlation coefficients ($R^2 > 0.57$) are obtained for all major cruises that sampled Fe-limited phytoplankton in several locations (Fig. 3), and for the entire dataset with 560 single-cell data points (SI section S3).

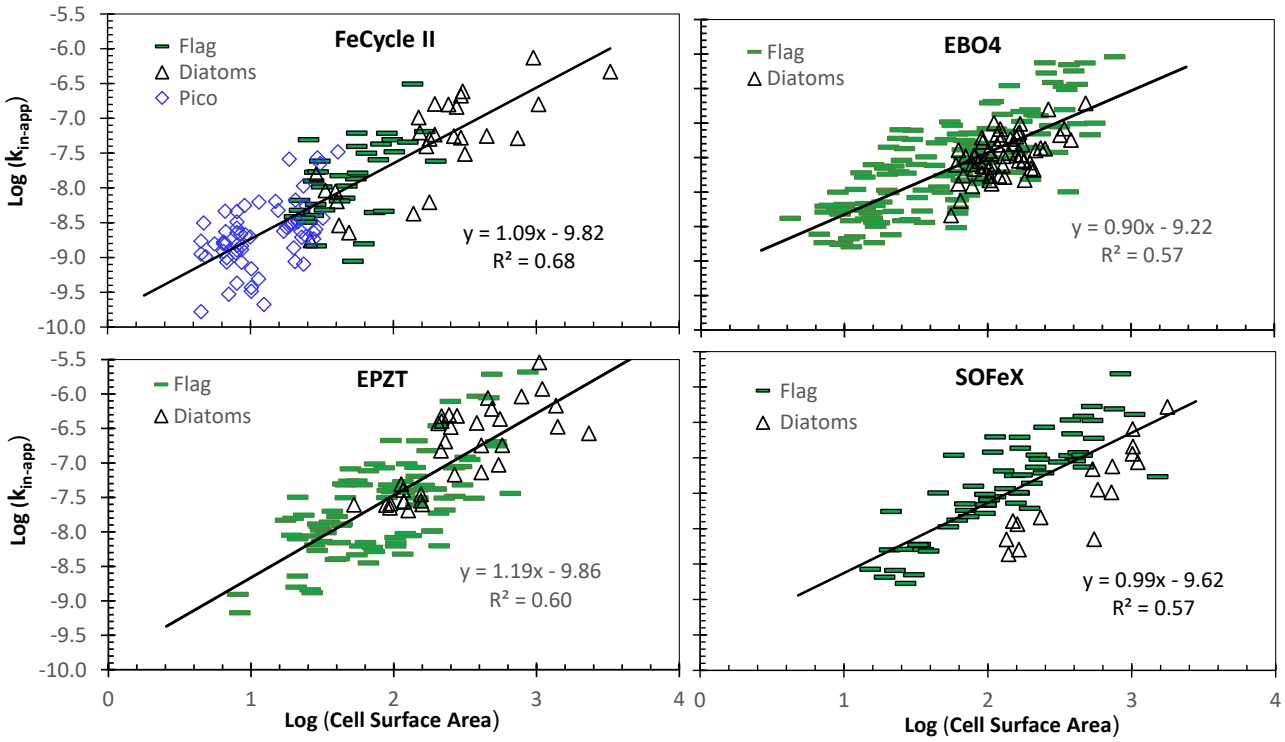

Figure 3. Proportionality between $k_{in\text{-}app}$ of individual cells (L cell^{-1} d^{-1}) and their respective cell surface area (μm^2). Logged data from several cruises: A. FeCycle II, B. EB04, C. EPZT, and D. SOFeX. Scales are identical for all graphs and major cell types are shown as different symbols. Tight proportionality between $k_{in\text{-}app}$ and cell surface area is deduced from the near unity (1) slope values and the high correlation coefficients (See SI section S3 for further details).

The linear relationship between $k_{in\text{-}app}$ and S.A. suggests that, across these broad oceanic regions, Fe-limited cells are subjected to similar constraints on available membrane-space for Fe transport, and can thus provide a common indicator of dFe availability. Subsequently, we normalize $k_{in\text{-}app}$ to cell S.A., and propose the resulting parameter as a measure of dFe bioavailability:

Eq. 2: Bioavailability of SW dFe (L μm^{-2} d^{-1}) = $k_{in\text{-}app}$ (L $cell^{-1}$ d^{-1}) / S.A. (μm^2 $cell^{-1}$)

3.3 Consistency of $k_{in\text{-}app}$/S.A. among different degrees of Fe-limitation

The degree of Fe-limitation, as deduced from measured dFe concentrations, physiological and molecular Fe-deficiency markers, and grow-out incubations, varies substantially among sites (Table 1). Moreover, at any given station, different species of phytoplankton may experience varying degrees of Fe-limitation, depending on their size, life history, Fe acquisition mechanisms, Fe-requirements and Fe-use efficiencies (Fourquez et al., 2020; Maldonado et al., 2005; Twining et al., 2021). Hence, $k_{in\text{-}app}$/S.A. should remain constant across varying degrees of Fe-limitation for it to provide a reliable measure of dFe availability.

Laboratory studies have shown that, once the activity of the high-affinity Fe uptake system has been maximized, Fe uptake rate constants remain largely unchanged at varying degrees of Fe-limitation (Kustka et al., 2007; Lis et al., 2015b; Maldonado & Price, 2001). Cellular Fe stress is expected to occur when dFe < $K_{\mu Q}$, the half-saturation constant of steady-state Fe uptake, estimated at ca. 0.8 nM (Marchetti and Maldonado, 2016). High-affinity Fe uptake mechanisms should be expressed even when macronutrients are low, as shown by Caputi et al. (2019) for ISIP gene expression in the sub-tropical Pacific gyres. Thus, $k_{in\text{-}app}$/S.A. should provide a valid estimate of Fe uptake rates across all low-Fe systems. Matching these expectations, average $k_{in\text{-}app}$/S.A. did not differ in populations estimated *a priori* to be either mildly or strongly Fe-limited (Fig. 4). Among Fe-limited populations, $k_{in\text{-}app}$/S.A. shows no statistically significant relationship with dFe. Geometric mean $k_{in\text{-}app}$/S.A. across these Fe-limited populations was $3.16 \pm 0.82 \times 10^{-10}$ L μm^{-2} d^{-1} (± 95% CI; Fig. 4). In contrast, $k_{in\text{-}app}$/S.A. was about 10-fold lower in populations that were either Fe replete or limited by N ($p < 0.0001$; Fig. 4). Such a drop in $k_{in\text{-}app}$/S.A. matches expectations, since Fe-replete cells downregulate their high affinity Fe transport systems and reduce the density of Fe-transporters on the cell surface (Hudson & Morel, 1993; Maldonado & Price, 2001). This supports our assertion that Fe bioavailability can be assessed at all stations where high-affinity Fe uptake systems are being maximized (dFe < 0.6 nM).

Given the broad use of N/Fe as a Fe-limitation index (as we have done above) and the recognition that large ocean regions may be co-limited by N and Fe (Browning et al., 2017), it is interesting to also consider the applicability of $k_{in\text{-}app}$/S.A. in low-N areas. Our Fe-uptake constant does appear to vary as a function of $\log_{10}$(N/Fe) (Fig. S5), however this relationship is driven by N-availability controls on phytoplankton growth rates that are independent of Fe availability. There is no relationship between $k_{in\text{-}app}$/S.A. and $\log_{10}$(N/Fe) when the low-N stations (represented by X's and white symbols in Figs. 4 and S5) are removed. Thus, our approach to calculating $k_{in\text{-}app}$/S.A. cannot be applied in regions where macronutrient availability limits growth rates, as Fe uptake and cell growth is decoupled in these systems (Twining et al., 2021). The disconnect can be seen in Fig. 4, where calculated $k_{in\text{-}app}$/S.A. are ca. 10-fold below those calculated for cells not limited by N. However, the calculated geometric mean $k_{in\text{-}app}$/S.A. should be applicable to regions with low N and low Fe, as high-affinity Fe uptake appears to occur in low-Fe areas independent of N availability (Caputi et al., 2019).

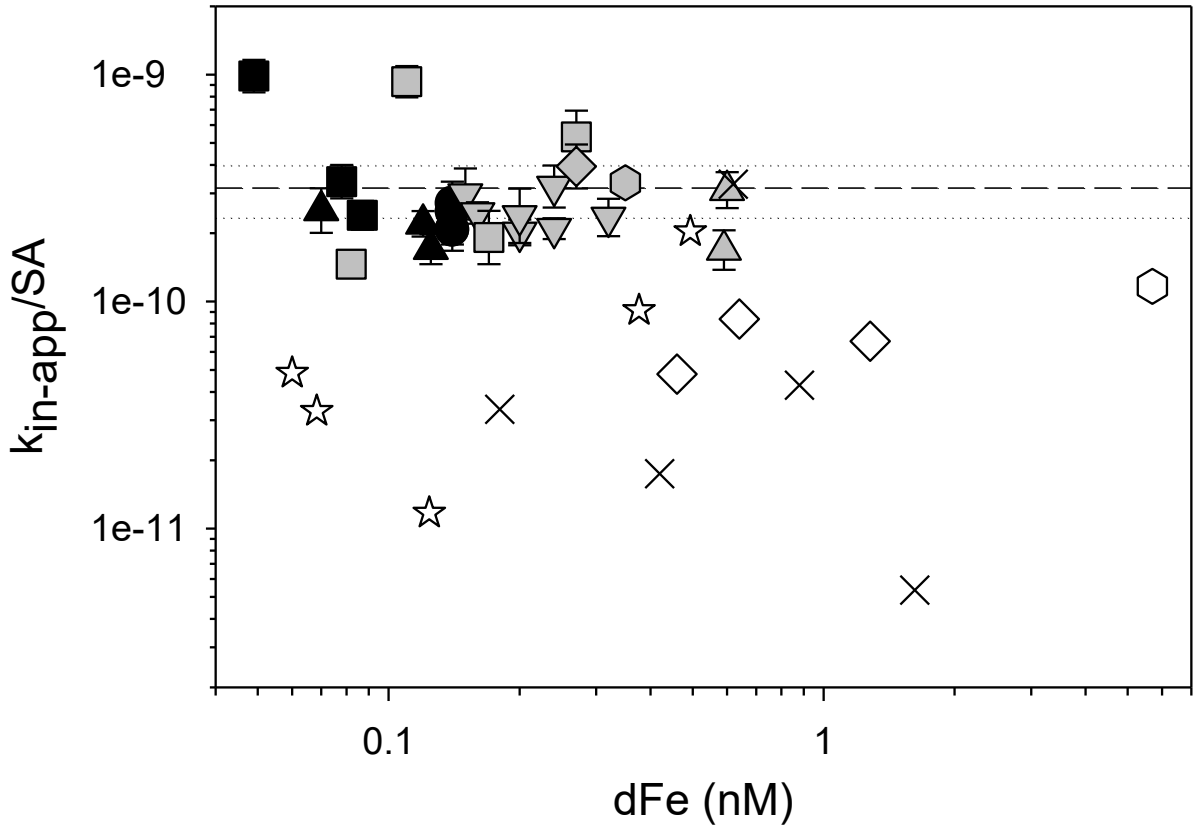

Figure 4. Station-average $k_{in\text{-}app}$/S.A. (surface area normalized dFe uptake rate constant), plotted against dissolved Fe concentrations. The Fe-limitation status of the population is indicated by symbol shading (black: strong Fe limitation, gray: mild Fe limitation, white: no primary Fe limitation). Symbols are means ± SE for all cells at the Fe-limited stations. Dashed and dotted lines indicated geometric mean and 95% CI $k_{in\text{-}app}$/S.A. across all Fe-limited stations. Symbols for individual cruises are: SOFeX—circle, FeCycle II – triangle, EB04 – inverted triangle, EPZT – square, GeoMICS – diamond, IrnBru – hexagon, IO9N – star, NAZT – X.

3.4 Consistency of $k_{in\text{-}app}$/S.A. among phytoplankton groups

The dataset contains cells from different groups, which were broadly categorized as diatoms, flagellates and picoeukaryotes (Table 1). For $k_{in\text{-}app}$/S.A. to provide a reliable measure of dFe availability, the differences among these groups should be small. Shaked et al., (2020) reported a similarity in $k_{in\text{-}app}$/S.A. among several cultured species from different taxa, based on short-term uptake experiments with natural seawater. Here, however, $k_{in\text{-}app}$/S.A. is calculated using cell Fe quotas, which differ between phytoplankton groups (Twining & Baines, 2013, Twining et al., 2021).

Acknowledging the possible variations in $k_{in\text{-}app}$/S.A. among natural communities, we examined the four low-Fe studies for which more than one cell type was analyzed. In FeCycle II and EB04 cruises, diatoms, flagellates and picoeukaryotes had mostly comparable $k_{in\text{-}app}$/S.A. (Fig. 3, Fig. S6). Stronger taxonomic group differences were seen in SOFeX, where least-squares geometric mean diatom $k_{in\text{-}app}$/S.A. (0.51×10^{-10} L μm^{-2} d^{-1}) was only 16% of that observed in flagellates (3.1×10^{-10} L μm^{-2} d^{-1}; Fig. 3d, Fig. S6). This difference likely reflects the markedly lower Fe quota-

to-volume ratios that can be achieved by Fe-limited Southern Ocean diatoms (Strzepek et al., 2011). In contrast, diatoms in the EPZT cruise had 1.7 times higher $k_{in\text{-}app}$/S.A. than those of flagellates (5.0 vs 2.9 x 10^{-10} L μm^{-2} d^{-1}, Fig. S6), possibly reflecting the Fe-storage capacity of some diatoms, especially under differential N and/or Si limitation (De La Rocha et al., 2000; Twining et al., 2021).

Combining these 4 studies, we found statistically significant but relatively minor (~1.4 fold) differences in $k_{in\text{-}app}$/S.A. between cell types (SI section S5). Least-square geometric mean $k_{in\text{-}app}$/S.A. were 2.1 x 10^{-10}, 3.0 x 10^{-10}, and 2.2 x 10^{-10} L μm^{-2} d^{-1} for diatoms, flagellates, and picoeukaryotes, respectively. The variations in phytoplankton taxa $k_{in\text{-}app}$/S.A. likely reflect unique physiologies related to Fe-sparing and Fe-storage strategies. But, these taxon differences are small relative to the overall variance in station-specific $k_{in\text{-}app}$/S.A. across all stations (~5 fold, Table 1), and hence will exert at most a marginal effect on comparisons of dFe bioavailability.

3.5 Comparing $k_{in\text{-}app}$/S.A. among cruises and former studies and implications for oceanic dFe availability

Having confirmed that $k_{in\text{-}app}$/S.A. is a valid standardized proxy for bioavailability, we further explore the dataset to gain insights on the availability of dFe in the ocean. We compare uptake constants of both individual cells (Fig. 5a) and geometric means of discrete stations (Fig. 5b) among the various research campaigns. These are further compared to the bioavailability envelope that empirically predicts the upper and lower limits of Fe availability to phytoplankton in seawater (Lis et al., 2015b). The upper black line in Fig. 5 represents the most bioavailable Fe species - Fe′, while the lower green line, the least bioavailable Fe species – FeDFB. The space between them defines the bioavailability envelope, where all Fe-complexes are predicted to reside. We also plot the average uptake rate constant of seawater dFe as probed by Fe-limited laboratory cultures (Fig. 5b, Shaked et al., 2020).

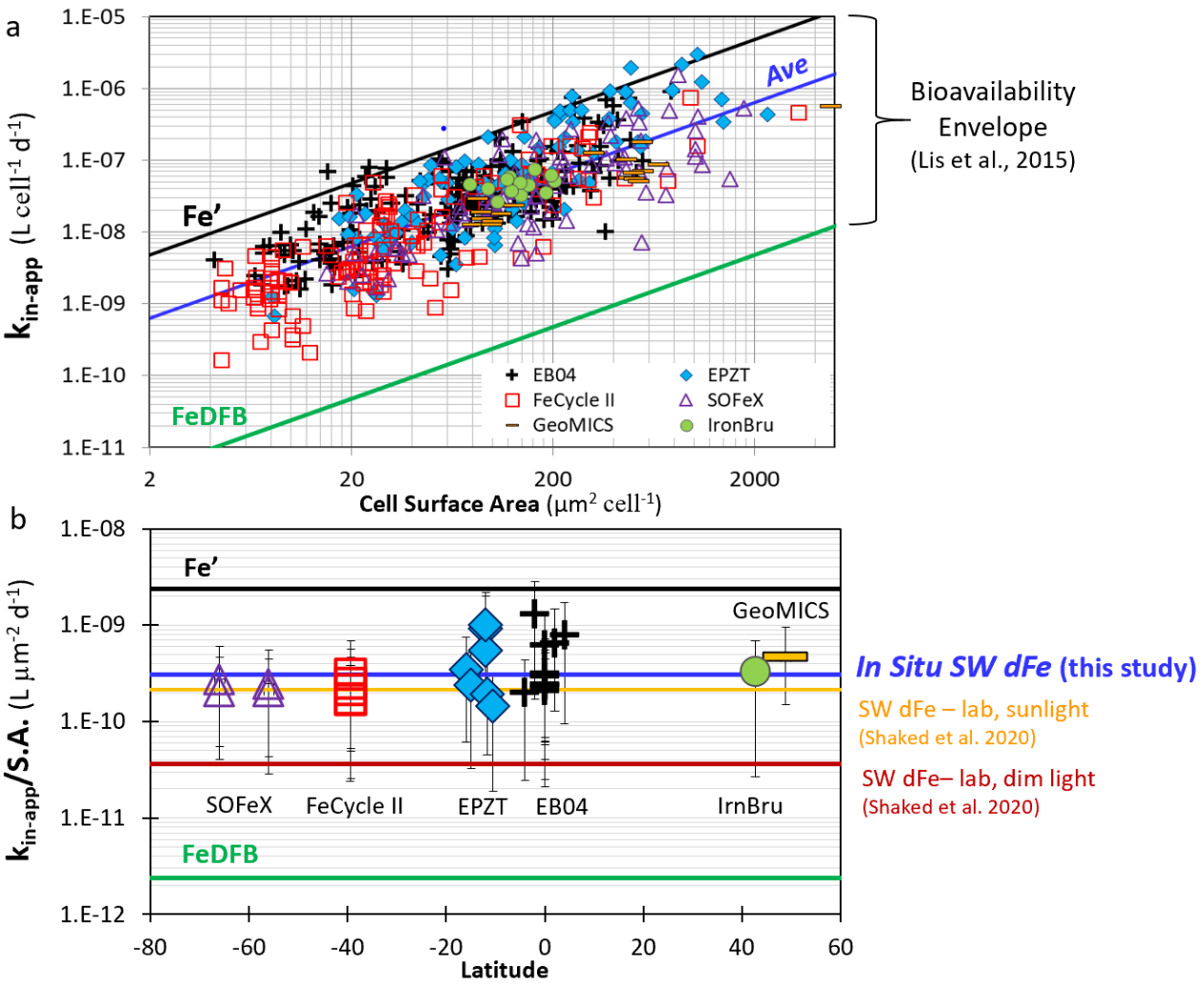

Figure 5. Summary of dFe bioavailability proxy (k_{in-app}/S.A.) obtained in this study, shown individually for 560 single Fe-limited cells (a) and averaged (geometric means) per station (b). These values were obtained for Fe-limited phytoplankton from 6 different ocean regions, with temperatures ranging from -0.7ºC to 26ºC, and dFe concentrations spanning from 0.05 to 0.6 nM (Fig. 1, Table 2). The 'bioavailability envelope' predicted from laboratory cultures with defined Fe-complexes (Lis et al., 2015b) is plotted for comparison (k_{in}/S.A = 2.4 x 10^{-9} and 2.4 x 10^{-12} L µm^{-2} d^{-1} for Fe′ and DFB, respectively). Also shown are estimates of dFe bioavailability of natural seawater probed by cultured Fe-limited phytoplankton (Shaked et al., 2020), under either dim or natural light (k_{in-app}/S.A = 3.6 x 10^{-11} and 2.1 x 10^{-10} L µm^{-2} d^{-1}, respectively). The grand mean dFe availability calculated here is plotted as a blue line (k_{in-app}/S.A = 3.2 ± 0.82 x 10^{-10} L µm^{-2} d^{-1}).

Significant scatter among individual-cell data is observed on a log-log plot of k_{in-app} versus S.A., yet none of the cruises stand out compared to the others (Fig. 5a). All values plot within the boundaries of the bioavailability envelope, clustering towards the upper range of the envelope, nearer to Fe′ than to FeDFB. This indicates that, as a whole, the availability of the mixed pool of Fe-complexes in seawater is much higher than that of strong Fe-siderophore complexes. In fact, based on our data, we can set a new lower limit of dFe availability in the ocean, which is ~10 fold higher than that defined by the non-photo-labile siderophore FeDFB. Although Fe-binding ligands in the ocean generally have strong complexation constants that are comparable to model siderophores (Gledhill & Buck 2012), dFe availability in the ocean is significantly higher than for

Fe bound to these siderophores. This is likely due to a number of rapid physiological and photochemical Fe cycling processes that occur in natural systems. These processes appear to increase the availability of dFe species by generating the highly bioavailable Fe′ (Barbeau et al., 2001; Maldonado & Price, 2001; Maldonado et al., 2005; Shaked, 2008; Waite, 2001).

Geometric means of $k_{in\text{-}app}$/S.A. at discrete stations spanning a broad geographical range and temperature gradient were rather consistent, generally 2-5 x 10^{-10} L μm^{-2} d^{-1} (Fig. 5b). Higher values are found in some of the Equatorial Pacific stations from EB04 and EPZT cruises, which may be due to poorly-constrained dFe (for some EB04 stations where measured dFe approached analytical capabilities; (Kaupp et al., 2011) or taxon-specific Fe storage at some EPZT stations (Twining et al., 2021)). Nonetheless, focusing on the consistency among most stations, we computed averaged oceanic dFe availability ($k_{in\text{-}app}$/S.A.) of 3.16 ± 0.82 x 10^{-10} L μm^{-2} d^{-1} (mean ± 95% confidence interval). This exceeds the value estimated from cultures under dim laboratory light (Fig. 5b, red line), but agrees well with outdoors experiments where photochemical reactions increase dFe availability (Fig. 5b orange line; Shaked et al., 2020). The close match between $k_{in\text{-}app}$/S.A. of phytoplankton from culture and the ocean suggests that photochemical reactions in the surface ocean are important to increase dFe bioavailability by temporarily releasing inorganic Fe (Fe′) from Fe-complexes. Cells analyzed in this study were collected from the upper 20 meters of the water column where some of the Fe-complexes undergo photochemical degradation to form the highly labile but short-lived Fe′.

4. Discussion

The surface area-normalized uptake rate constant ($k_{in\text{-}app}$/S.A.) derived above met all pre-defined criteria. It is proportional to cell surface area and broadly consistent across diverse phytoplankton communities from low-Fe ocean regions that experience various degrees of Fe limitation. It thus can serve as a proxy of oceanic dFe bioavailability in near-surface waters of lowFe regions. The grand average $k_{in\text{-}app}$/S.A of 3.16 ± 0.82x 10^{-10} L μm^{-2} d^{-1}, which provides a first order estimate of a mean dFe bioavailability, agrees with previous, independent estimates and supports the significance of photochemistry in increasing dFe availability in surface waters. Comparison with the published Fe bioavailability envelope indicates that, indeed, most dFe in low-Fe ocean regions appears to be available for uptake by phytoplankton over relevant timescales. Note that our analysis reflects primarily conditions in near-surface waters of Fe-limited regions. Colloids, which were not directly considered in this analysis and may contribute to the dFe pool, could also potentially affect dFe availability; their significance likely increases with depth as they recycle through the photic zone (Boye et al., 2010).

To further apply our proxy, we next normalize it to carbon instead of surface area; this allows us to predict *in situ* Fe uptake rates and calculate biologically-driven residence times of dFe in the surface ocean. Lastly, we apply our uptake rate constants to constrain global model predictions regarding climate change impacts on primary productivity and upper trophic levels in the Fe-limited eastern equatorial Pacific.

4.1 Generating a carbon-normalized bioavailability proxy ($k_{in\text{-}app}$/C)

A potential drawback in the use of $k_{in\text{-}app}$/S.A. for assessing biological Fe uptake in ocean models is that phytoplankton surface area is rarely measured or incorporated in these models, which instead usually rely on cell C. Most experimental phytoplankton uptake data are obtained by

filtration onto specific pore size filters, and converting these data to S.A. introduces large uncertainty. In contrast, C uptake rates are often measured simultaneously with Fe uptake rates, which are then reported normalized to C or chlorophyll (Ellwood et al., 2020; King et al., 2012; Mellett et al., 2018). Hence a C-normalized bioavailability proxy - $k_{in\text{-}app}/C$, with units of L mol C^{-1} d^{-1}, would have wide application in experimental and modeling studies.

In the dataset analyzed in this study, cellular C quotas were estimated for each cell from calculated cell volumes using the carbon-to-volume relationships of Menden-Deuer and Lessard (2000). This allows a straightforward conversion of $k_{in\text{-}app}/S.A.$ to $k_{in\text{-}app}/C$, but there are some caveats to consider. For example, while cellular C is proportional to cellular volume, $k_{in\text{-}app}$ is proportional to S.A. (Fig. 3), and cell volume to S.A. ratios are not constant, varying according to cell shape and size. Moreover, carbon-to-volume relationships published by Menden-Deuer & Lessard (2000) differ between diatoms and non-diatoms. Despite these caveats, $k_{in\text{-}app}/S.A.$ is highly correlated with $k_{in\text{-}app}/C$, when comparing both individual cells and station averages (SI section S6).

Similar to $k_{in\text{-}app}$ /S.A., the C-normalized Fe bioavailability proxy shows only small variations among most individual stations in a single cruise and among cruises (Fig. 6). The calculated grand average (geometric mean) $k_{in\text{-}app}$ /C in our study is 42,200 ± 11,000 L mol C^{-1} d^{-1} (mean ± 95% confidence interval) well within the range reported for different regions using independent measurements (SI Table S3).

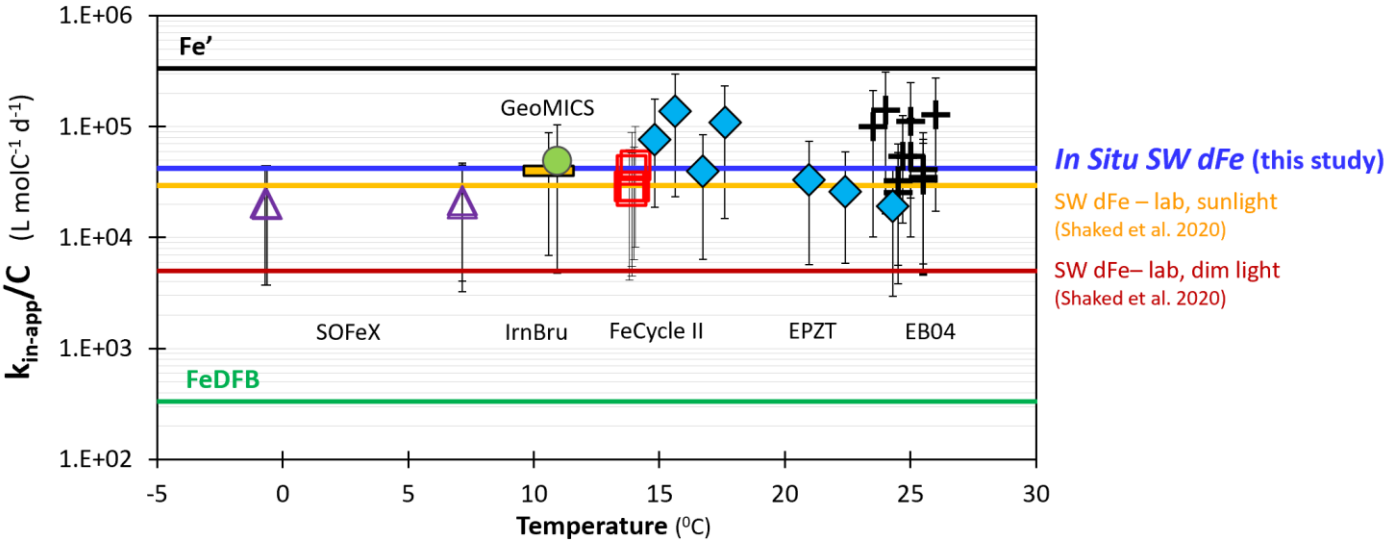

Figure 6. C-normalized Fe uptake constants for individual Fe-limited stations included in the dFe availability analysis. Rate constants are for the same stations as in Figure 5, but Fe uptake is normalized to cellular C rather than cell surface area. Symbols are geometric means ± SE for all of the cells at each station. The blue line indicates the geometric mean $k_{in\text{-}app}/C$ (42,200 ± 11,000 L molC^{-1} d^{-1}). As in Figure 5, the equivalent boundaries of the bioavailability envelope (Lis et al., 2015b) were plotted as well as average constants for natural seawater under dim and high light (Shaked et al., 2020). These reference values were converted from S.A. normalized to C-normalized values using the average C/S.A. relationship for all cells analyzed in this study (1.4×10^{14} µm^2 mol C^{-1}).

4.2 Applying $k_{in\text{-}app}/C$ to predict Fe uptake rates in the ocean

The C-normalized Fe-uptake constant can be used to calculate Fe uptake rates by phytoplankton communities using equation 3, and calculated rates can be compared to those measured directly *in situ*.

Eq 3. *In situ* Fe uptake rate (mol L^{-1} d^{-1}) =

$$k_{in\text{-}app}/C \text{ (L mol } C^{-1} \text{ } d^{-1}) \text{ x Cellular C or POC (mol } L^{-1}) \text{ x [dFe] (mol } L^{-1})$$

We selected studies that conducted on-deck Fe uptake experiments with natural phytoplankton communities using small additions of a radioactive tracer (typically 0.2 nM ^{55}Fe). We compared measured rates with rates calculated using the grand average $k_{in\text{-}app}/C$ (42,200 L $molC^{-1}$ d^{-1}), dFe concentrations in the experiment (i.e. ambient dFe + ^{55}Fe), and POC (particulate organic carbon, Fig. 7). For a study lacking POC measurements (Mellett et al., 2018), we used *chlorophyll a* (Chl) instead of POC and converted the Fe uptake constant to $k_{in\text{-}app}/Chl$ (0.176 L µg Chl^{-1} d^{-1}, SI section S6). Predicted uptake rates are in good match with rates measured in the California upwelling system (Mellet et al., 2018) and the Subarctic Pacific (King et al., 2012) , generally within 5-50% of measured values (Fig. 7, mean difference - 18±7%). In the Southern Ocean (Ellwood et al., 2020), predicted rates exceed measured rates, possibly reflecting the somewhat lower dFe availability in this region (perhaps driven by dimmer irradiance) in accord with lower than average $k_{in\text{-}app}/C$ found in SOFeX (20,400 ± 4000 L mol C^{-1} d^{-1}; Fig. 6, SI section S6).

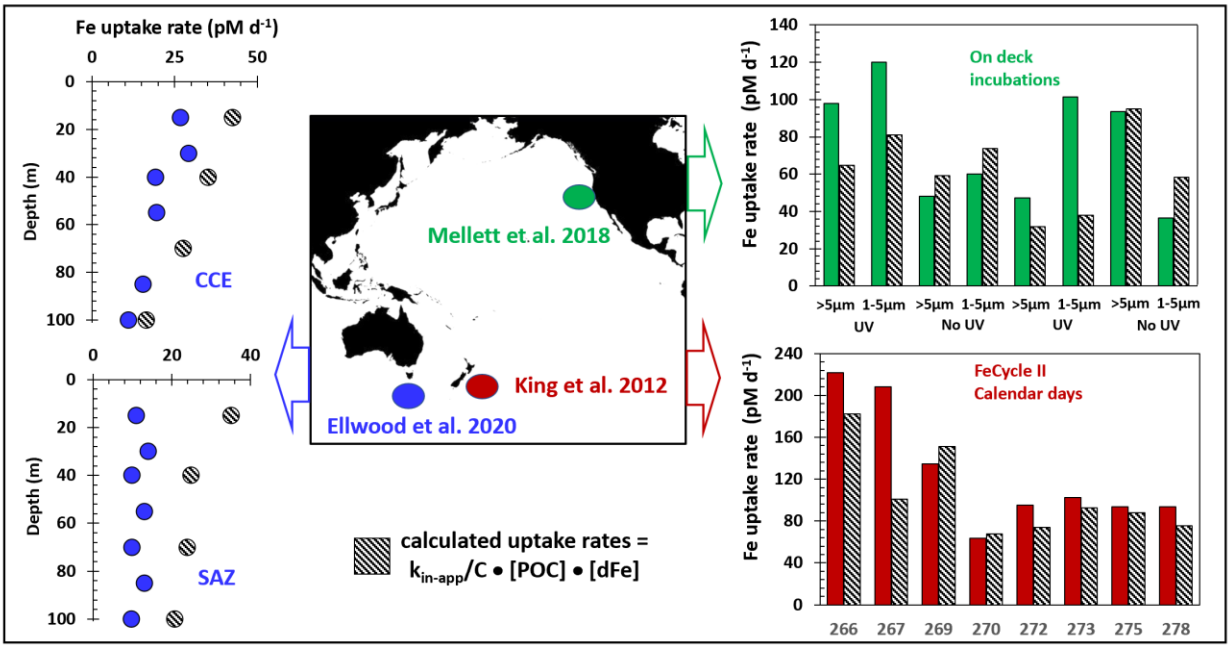

Figure 7. Application of the bioavailability proxy $k_{in\text{-}app}/C$ to calculate Fe uptake rates in the ocean. We compare uptake rates measured in several studies (colored bars) with uptake rates calculated according to Eq. 3 (hatched bars), using reported dFe and POC (or Chl). Studies are color coded: Blue – Ellwood et al., (2020) Green – Mellett et al., (2018), and Red- King et al., (2012).

The grand average biomass-normalized uptake rate constant ($k_{in\text{-}app}/C$) provides a simple means to derive Fe uptake rates from field data on a large spatial scale. In this way, our new insight into $k_{in\text{-}app}/C$ and Fe bioavailability can assist experimental design, data interpretation and modeling,

taking advantage of the growing number of the high quality dFe measurements generated through the GEOTRACES program.

However, care should be taken, as this approach applies only to Fe limited or stressed regions (where phytoplankton uptake systems are saturated). In addition, $k_{in\text{-}app}/C$ is derived from near-surface cells and may differ deeper in the euphotic zone due to variations in Fe speciation and cycling. Because of this, $k_{in\text{-}app}/C$ cannot be a simple replacement for the prognostic Fe uptake scheme in ocean models. These schemes require assumptions to be made around key parameters, like V_{max} and K_s, or feedbacks linked to up- and downregulation of Fe uptake that until now have been impossible to validate. However, $k_{in\text{-}app}/C$ can be easily derived from the model output (Fe uptake rate, Fe quota and dFe concentration), providing a unique way to assess the skill of modeled iron uptake rates in low Fe regions (see section 4.4).

The presence of a reasonably constant $k_{in\text{-}app}/C$ for diverse Fe-limited communities across the ocean suggests that there is an emergent limit to the uptake rates that can be realized by these communities. This may follow logically from the underlying concept that Fe uptake is limited by biological surface area available for Fe transporters at the cell surface, which are responsible for accumulating Fe into cell biomass. Iron-limitation also places constraints on cell size (and hence S.A./vol), since Fe uptake by large taxa will be diffusion-limited (Timmermans et al., 2001). Comparison of our $k_{in\text{-}app}$ values with estimated maximum diffusive fluxes of Fe′ and FeDFB (SI section S8), further demonstrates that cell surface/membrane space are restricting dFe uptake in the ocean, while diffusion limitation "kicks in" only for spherical cells greater than 60 μm in diameter (Fig. S10). The consistency of this parameter also suggests that these *communities* have maximized Fe uptake and thus approach the physiological limits measured for monocultures in the laboratory.

4.3 Applying $k_{in\text{-}app}/C$ to evaluate biologically-derived dFe residence times in low Fe surface waters

The C-normalized Fe uptake constant - $k_{in\text{-}app}/C$ - can help quantify Fe cycling by providing a simple estimate of biological-derived dFe residence time in the upper ocean. Typically, this time is estimated by dividing the Fe concentration (or inventory) by phytoplankton Fe uptake rates. Since Fe uptake rates have been measured only in a handful of studies, biological-derived dFe residence times are rarely estimated. Inserting equation 3 into the residence time calculation results in the following relationship:

Eq. 4: Biologically-derived dFe residence time (d) $= 1 / (k_{in\text{-}app}/C \text{ (L mol C}^{-1} \text{ d}^{-1}) \text{ x POC (mol L}^{1}))$

Equation 4 suggests that the timescales of biological Fe cycling in low Fe systems are a function of phytoplankton biomass (POC) but actually not of dFe. As above, since Fe uptake capabilities are maximized under Fe-limitation, rates of uptake (and hence residence times) are driven by biomass. POC levels in low-Fe regions are generally constrained between 2-10 μM (Bowie et al., 2001, 2015; Ellwood et al., 2020; King et al., 2012; Strzepek et al., 2005), resulting in predicted residence rates of 2.4-12 days. These estimates are very similar to residence times determined from direct measurements of Fe uptake and dFe in a range of low-Fe systems (SI Table S4), suggesting that our approach is robust.

These estimates of biologically-derived Fe residence times are notably shorter than published residence times for dFe in the upper ocean. Black et al., (2020) calculated Fe residence times for

major ocean basins by combining particulate Fe measurements with flux estimates from sediment traps and ^{234}Th disequilibrium. They found upper ocean residence times of dissolved Fe, relative to biological Fe export, to range broadly from a month to a decade, suggesting that dFe is cycled 10 or more times, on average, before being exported with sinking biomass. This supports previous assertions that productivity in most systems is supported by recycled Fe (Boyd et al., 2005, 2017) and points to the likely role of biological processes in driving the decoupling between iron and other nutrient cycles (Rafter et al., 2017).

4.4 Applying $k_{in\text{-}app}/C$ to constrain model simulations of Fe uptake rates

The observationally-derived uptake constant $k_{in\text{-}app}/C$ can also be used to evaluate Fe uptake rates predicted by numerical ocean models. Iron uptake rates in ocean models are poorly constrained observationally and result from model assumptions regarding a suite of poorly known parameters that represent the cellular affinity and storage capacity for Fe (e.g., Aumont et al., 2015; Stock et al., 2014). Additionally, ocean model performance is usually evaluated and compared via static metrics such as dFe concentrations and distributions, but this approach can belie significant differences in Fe cycling and residence times (Tagliabue et al., 2016) and lead to important uncertainties in the response of Fe limited regions to climate change (Tagliabue et al., 2020). Indeed, a recent effort to evaluate Fe fluxes in the Pacific Ocean concluded that small vertical gradients in dFe obscure easy detection of large, and often opposing, Fe flux terms (Tagliabue et al., 2019). Thus, to improve ocean Fe models requires the ability to evaluate their underlying fluxes, especially those linked to biology. The $k_{in\text{-}app}/C$ constant provides a first-order way to do this.

As an example of this application, we use $k_{in\text{-}app}/C$ to constrain model simulations assessing the impact of climate change on ocean productivity. Recently, Tagliabue et al. (2020) utilized a comprehensive set of model simulations to predict changes in net primary production (NPP) and upper trophic level biomass in the Eastern Equatorial Pacific under the high emissions RCP8.5 climate change scenario. Their simulations utilized scenarios of high or low Fe uptake, which differ only in the maximum uptake rate applied but lead to differences in the strength of Fe limitation in the upper ocean. Simulations using high or low Fe uptake rates performed similarly in the present day (1986-2005), but the future NPP projections differed markedly (Tagliabue et al., 2020).

This region overlaps the EB04 cruise included in this study, presenting an opportunity to assess the different model scenarios using our field-derived $k_{in\text{-}app}/C$. In Fig. 8, we plot EB04 cruise track, the observed $k_{in\text{-}app}/C$ of each station and the $k_{in\text{-}app}/C$ derived from the PISCES model. We first extracted for each station the modeled Fe uptake rates (present day runs). Then, re-arranging equation 3, we derived $k_{in\text{-}app}/C$ from these Fe uptake rates using cell quotas and dFe concentrations (all from the model).

Our field-derived $k_{in\text{-}app}/C$ clearly support the model scenario with lower Fe uptake (Fig. 8). The high Fe uptake model scenario shows $k_{in\text{-}app}/C$ that are much higher than EB04 observations, indicating that Fe bioavailability is overestimated in this model scenario. This unique assessment of the modeled biological Fe cycle suggests that the large decline in Equatorial Pacific NPP projected under the high Fe uptake scenario would be less likely to occur (Tagliabue et al., 2020) and highlights the usefulness of our observational based constant for constraining global ocean model predictions. Moreover, this exercise illustrates a means to widely assess the fidelity of

modeled phytoplankton Fe uptake for Fe-limited regions across a wide range of available earth system models. In doing so, a novel constraint on the biological Fe cycle component of these models would be provided, which complements the common assessments against bulk properties, such as dFe or chlorophyll.

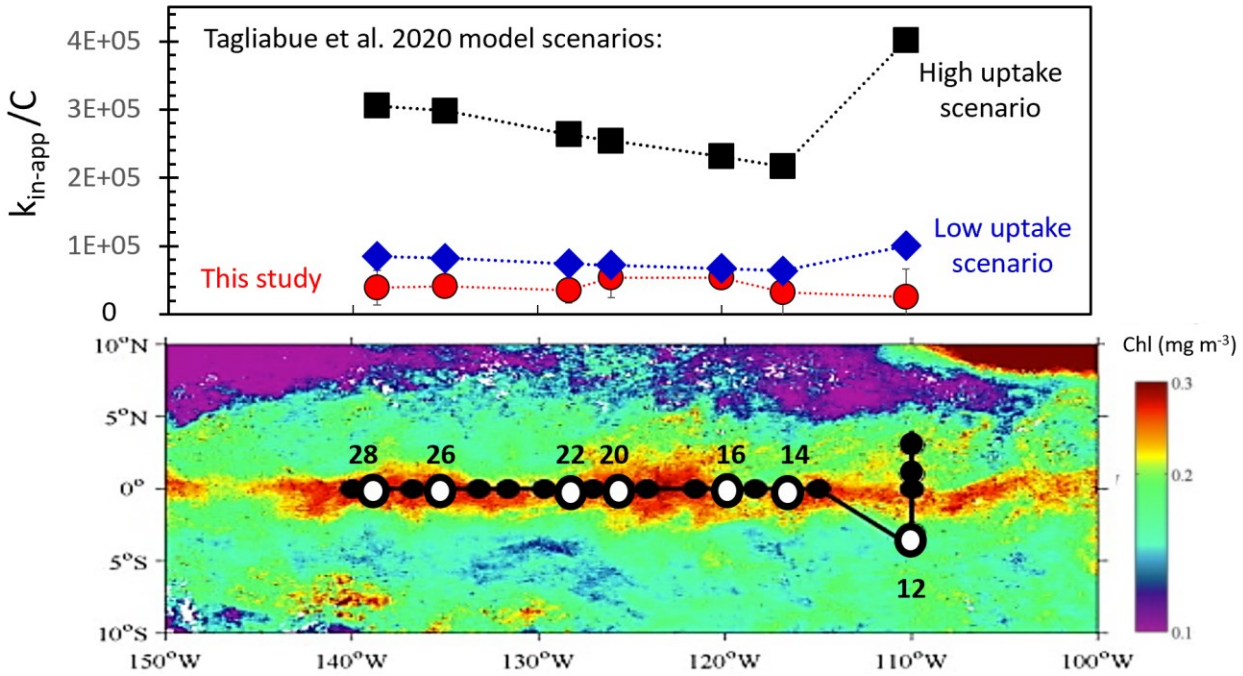

Fig. 8 Utilization of k_{in-app}/C values to constrain model predictions for the equatorial Pacific Ocean. In the upper panel, red circles show the average k_{in-app}/C of low-Fe stations from the EB04 cruise along the equator. Stations with dFe below the detection limit have been removed. The black and blue symbols show k_{in-app}/C derived from uptake rates used in the model of Tagliabue et al., (2020), corresponding to the stations location. The model was run assuming either high uptake scenarios (black squares) and or low uptake scenarios (blue diamonds). In the lower panel, the cruise track was plotted over satellite-measured chlorophyll (Chl, from Brzezinski et al., 2011), and relevant stations are highlighted in white circles, with cruise station numbers indicated.

5. Conclusions

In this study we quantified dFe bioavailability in the ocean by examining Fe uptake rate constants of *in situ* eukaryotic phytoplankton. To do so, we combined Fe quotas of 930 natural cells measured with synchrotron X-ray fluorescence, with modeled growth rates, and calculated *in situ* steady-state Fe uptake rates for single cells from diverse oceanic regions. We then divided these rates by concurrently-measured dFe concentrations to estimate *in situ* Fe uptake rate constants (k_{in-app}). These k_{in-app} were normalized to surface area or cellular C to derive k_{in-app} /S.A. or k_{in-app} /C, respectively. The surface area normalized uptake rate constants (k_{in-app} /S.A.) show that cells in low-Fe systems have higher Fe uptake rate constants than cells in Fe-replete or N-limited systems, as expected from physiological studies. In order to use k_{in-app} as a proxy of dFe bioavailability,

only $k_{in\text{-}app}$ for Fe-limited or Fe-stressed cells were included, reducing our dataset to 560 $k_{in\text{-}app}$ values.

Focusing on Fe-limited / Fe-stressed regions, we observed that the surface area normalized uptake rate constants ($k_{in\text{-}app}$/S.A.) varied by ~5 fold, over a broad latitudinal range, indicating consistent behavior across Fe-limited regions and enabling us to estimate a grand average Fe uptake rate constant for low Fe regions. Compared to specific Fe-complexes and species in seawater, the averaged seawater dFe availability is significantly higher than non-photolabile siderophore-bound Fe, and somewhat lower than inorganic Fe′. The oceanic near-surface $k_{in\text{-}app}$/S.A. values agree well with cultured-based estimates measured under natural sunlight, highlighting the importance of photochemical transformation of dFe in the well-lit surface waters for dFe bioavailability.

Other applications of these *in situ* dFe uptake rate constants, especially when normalized to cell C, were also illustrated, as we used the $k_{in\text{-}app}$ /C to: a) validate predictions from an ocean models; and b) calculate biologically-derived Fe residence times in euphotic zones. Furthermore $k_{in\text{-}app}$ /C can be utilized to estimate Fe uptake rates in remote Fe-limited systems for which POC and growth rates can be inferred from remote sensing (Tanioka et al., 2020). In the future, our Fe bioavailability proxy can be applied, alongside the growing database of phytoplankton cellular Fe quotas (Twining et al., 2021), to provide novel constraints on the biological Fe cycle component of earth system models in Fe-limited systems, which can improve the predictability of the response of upper ocean productivity to climate change.

Acknowledgments, Samples, and Data

We thank Robert Anderson for initiating this research during the GEOTRACES/OCB joint workshop on internal cycling of trace metals in the ocean held at Lamont-Doherty Earth Observatory in 2016, and for his endless encouragement and insights since. We acknowledge the valuable contributions of Rob Middag, Zanna Chase, Dan Repeta, Bill Sunda, Chen Zeng, Phoebe Lam and Seth John for dFe analysis, data interpretation and discussions. Sara Rauschenberg calculated surface areas for each of the analyzed cells. We thank Marion Fourquez and Viena Puigcorbé for sharing their unpublished data. This work was supported in part by Israel Science Foundation (www.isf.org.il) grant 458/15 and the German–Israeli Foundation for Scientific Research and Development (www.GIF.org.il) grant 1349 awarded to Y.S, as well as a Canadian NSERC grant awarded to M.M. Additional support came from US National Science Foundation grants OCE-1232814, OCE-1435862, and 1829819 awarded to BST. A.T. received funding from the European Research Council (ERC) under the European Union's Horizon 2020 research and innovation programme (grant agreement no. 724289). The work of SCOR working group 151 presented in this paper results, in part, from funding provided by national committees of the Scientific Committee on Oceanic Research (SCOR) and from a grant to SCOR from the U.S. National Science Foundation (OCE-1840868).

We hereby declare that none of the authors hold real or perceived financial conflicts of interests.

Data Availability Statement

All data used in our analysis has been previously published and the original studies have been cited in the body of the manuscript. These data are available from the Biological and Chemical Oceanography Data Management Office (BCO-DMO) in the following datasets:

https://www.bco-dmo.org/dataset/643270, https://www.bco-dmo.org/dataset/841640, https://www.bco-dmo.org/dataset/841583, https://www.bco-dmo.org/dataset/549122, https://www.bco-dmo.org/dataset/768064.

References

Allen, A. E., LaRoche, J., Maheswari, U., Lommer, M., Schauer, N., Lopez, P. J., … Bowler, C. (2008). Whole-cell response of the pennate diatom Phaeodactylum tricornutum to iron starvation. *Proceedings of the National Academy of Sciences of the United States of America*, *105*(30), 10438–10443. https://doi.org/10.1073/pnas.0711370105

Anderson, R. F. (2020). GEOTRACES: Accelerating Research on the Marine Biogeochemical Cycles of Trace Elements and Their Isotopes. *Annual Review of Marine Science*, *12*(1), 49–85. https://doi.org/10.1146/annurev-marine-010318-095123

Aumont, O., Ethé, C., Tagliabue, A., Bopp, L., & Gehlen, M. (2015). PISCES-v2: An ocean biogeochemical model for carbon and ecosystem studies. *Geoscientific Model Development*, *8*(8), 2465–2513. https://doi.org/10.5194/gmd-8-2465-2015

Baer, S. E., Rauschenberg, S., Garcia, C. A., Garcia, N. S., Martiny, A. C., Twining, B. S., & Lomas, M. W. (2019). Carbon and nitrogen productivity during spring in the oligotrophic Indian Ocean along the GO-SHIP IO9N transect. *Deep-Sea Research Part II: Topical Studies in Oceanography*. https://doi.org/10.1016/j.dsr2.2018.11.008

Barbeau, K., Rue, E. L., Bruland, K. W., & Butler, A. (2001). Photochemical cycling of iron in the surface ocean mediated by microbial iron(III)-binding ligands. *Nature*, *413*(6854), 409–413. https://doi.org/10.1038/35096545

Black, E. E., Kienast, S. S., Lemaitre, N., Lam, P. J., Anderson, R. F., Planquette, H., … Buesseler, K. O. (2020). Ironing Out Fe Residence Time in the Dynamic Upper Ocean. *Global Biogeochemical Cycles*, *34*(9). https://doi.org/10.1029/2020GB006592

Boiteau, R. M., Mende, D. R., Hawco, N. J., McIlvin, M. R., Fitzsimmons, J. N., Saito, M. A., … Repeta, D. J. (2016). Siderophore-based microbial adaptations to iron scarcity across the eastern Pacific Ocean. *Proceedings of the National Academy of Sciences*, *113*(50), 14237–14242. https://doi.org/10.1073/pnas.1608594113

Boiteau, R. M., Till, C. P., Coale, T. H., Fitzsimmons, J. N., Bruland, K. W., & Repeta, D. J. (2018). Patterns of iron and siderophore distributions across the California Current System. *Limnology and Oceanography*, *64*(1), 376–389. https://doi.org/10.1002/lno.11046

Bowie, A. R., Maldonado, M. T., Frew, R. D., Croot, P. L., Achterberg, E. P., Mantoura, R. F. C., … Boyd, P. W. (2001). The fate of added iron during a mesoscale fertilisation experiment in the Southern Ocean. *Deep-Sea Research Part II-Topical Studies in Oceanography*, *48*(11–12), 2703–2743.

Bowie, A. R., Van Der Merwe, P., Quéroué, F., Trull, T., Fourquez, M., Planchon, F., … Blain, S. (2015). Iron budgets for three distinct biogeochemical sites around the Kerguelen Archipelago (Southern Ocean) during the natural fertilisation study, KEOPS-2. *Biogeosciences*, *12*(14), 4421–4445. https://doi.org/10.5194/bg-12-4421-2015

Boyd, P. W., Law, C. S., Hutchins, D. A., Abraham, E. R., Croot, P. L., Ellwood, M., … Wilhelm, S. W. (2005). FeCycle: Attempting an iron biogeochemical budget from a mesoscale SF(6) tracer experiment in unperturbed low iron waters. *Global Biogeochemical Cycles*, *19*(4), 1–13. https://doi.org/Gb4s2010.1029/2005gb002494

Boyd, Philip W., Ellwood, M. J., Tagliabue, A., & Twining, B. S. (2017). Biotic and abiotic retention,

recycling and remineralization of metals in the ocean. *Nature Geoscience*, Vol. 10, pp. 167–173. https://doi.org/10.1038/ngeo2876

Boyd, Philip W., Strzepek, R., Chiswell, S., Chang, H., DeBruyn, J. M., Ellwood, M., … Hutchins, D. A. (2012). Microbial control of diatom bloom dynamics in the open ocean. *Geophysical Research Letters*, *39*(17). https://doi.org/10.1029/2012GL053448

Boye, M., Nishioka, J., Croot, P., Laan, P., Timmermans, K. R., Strass, V. H., … de Baar, H. J. W. (2010). Significant portion of dissolved organic Fe complexes in fact is Fe colloids. *Marine Chemistry*, *122*(1), 20–27. https://doi.org/10.1016/j.marchem.2010.09.001

Browning, T. J., Achterberg, E. P., Rapp, I., Engel, A., Bertrand, E. M., Tagliabue, A., & Moore, C. M. (2017). Nutrient co-limitation at the boundary of an oceanic gyre. *Nature*, *551*(7679), 242–246. https://doi.org/10.1038/nature24063

Bruland, K. W., Rue, E. L., & Smith, G. J. (2001). Iron and macronutrients in California coastal upwelling regimes: Implications for diatom blooms. *Limnology and Oceanography*, *46*(7), 1661–1674.

Brzezinski, M. A., Baines, S. B., Balch, W. M., Beucher, C. P., Chai, F., Dugdale, R. C., … Twining, B. S. (2011). Co-limitation of diatoms by iron and silicic acid in the equatorial Pacific. *Deep-Sea Research Part II: Topical Studies in Oceanography*, *58*(3–4), 493–511. https://doi.org/10.1016/j.dsr2.2010.08.005

Buck, K. N., Sedwick, P. N., Sohst, B., & Carlson, C. A. (2018). Organic complexation of iron in the eastern tropical South Pacific: Results from US GEOTRACES Eastern Pacific Zonal Transect (GEOTRACES cruise GP16). *Marine Chemistry*, *201*, 229–241. https://doi.org/10.1016/j.marchem.2017.11.007

Buck, K. N., Sohst, B., & Sedwick, P. N. (2015). The organic complexation of dissolved iron along the U.S. GEOTRACES (GA03) North Atlantic Section. *Deep-Sea Research Part II: Topical Studies in Oceanography*, *116*, 152–165. https://doi.org/10.1016/j.dsr2.2014.11.016

Bundy, R. M., Biller, D. V., Buck, K. N., Bruland, K. W., & Barbeau, K. A. (2014). Distinct pools of dissolved iron-binding ligands in the surface and benthic boundary layer of the California current. *Limnology and Oceanography*, *59*(3), 769–787. https://doi.org/10.4319/lo.2014.59.3.0769

Bundy, R. M., Boiteau, R. M., McLean, C., Turk-Kubo, K. A., McIlvin, M. R., Saito, M. A., … Repeta, D. J. (2018). Distinct Siderophores Contribute to Iron Cycling in the Mesopelagic at Station ALOHA. *Frontiers in Marine Science*, (5), 61. https://doi.org/10.3389/fmars.2018.00061

Cabanes, D. J. E., Blanco-Ameijeiras, S., Bergin, K., Trimborn, S., Völkner, C., Lelchat, F., & Hassler, C. S. (2020). Using Fe chemistry to predict Fe uptake rates for natural plankton assemblages from the Southern Ocean. *Marine Chemistry*, *225*. https://doi.org/10.1016/j.marchem.2020.103853

Caputi, L., Carradec, Q., Eveillard, D., Kirilovsky, A., Pelletier, E., Pierella Karlusich, J. J., … Iudicone, D. (2019). Community-Level Responses to Iron Availability in Open Ocean Plankton Ecosystems. *Global Biogeochemical Cycles*, *33*(3). https://doi.org/10.1029/2018GB006022

Coale, K. H., Johnson, K. S., Chavez, F. P., Buesseler, K. O., Barber, R. T., Brzezinski, M. A., … Johnson, Z. I. (2004). Southern Ocean Iron Enrichment Experiment: Carbon Cycling in High- and Low-Si Waters. *Science*. https://doi.org/10.1126/science.1089778

Cohen, N. R., Mann, E., Stemple, B., Moreno, C. M., Rauschenberg, S., Jacquot, J. E., … Marchetti, A.

(2018). Iron storage capacities and associated ferritin gene expression among marine diatoms. *Limnology and Oceanography*. https://doi.org/10.1002/lno.10800

Cutter, G., Andersson, P., Codispoti, L., Croot, P., Place, P., Hoe, T., … Obata, H. (2017). *Sampling and Sample-handling Protocols for GEOTRACES Cruises, version 3.0 ed.*

De La Rocha, C. L., Hutchins, D. A., Brzezinski, M. A., & Zhang, Y. H. (2000). Effects of iron and zinc deficiency on elemental composition and silica production by diatoms. *Mar. Ecol. Prog. Ser.*, *195*, 71–79.

Dreux Chappell, P., Virginia Armbrust, E., Barbeau, K. A., Bundy, R. M., Moffett, J. W., Vedamati, J., … Jenkins, B. D. (2019). Patterns of diatom diversity correlate with dissolved trace metal concentrations and longitudinal position in the northeast Pacific coastal−offshore transition zone. *Marine Ecology Progress Series*, *609*, 69–86. https://doi.org/10.3354/meps12810

Ellwood, M. J., Nodder, S. D., King, A. L., Hutchins, D. A., Wilhelm, S. W., & Boyd, P. W. (2014). Pelagic iron cycling during the subtropical spring bloom, east of New Zealand. *Marine Chemistry*, *160*, 18–33. https://doi.org/10.1016/j.marchem.2014.01.004

Ellwood, M. J., Strzepek, R. F., Strutton, P. G., Trull, T. W., Fourquez, M., & Boyd, P. W. (2020). Distinct iron cycling in a Southern Ocean eddy. *Nature Communications*, *11*(1). https://doi.org/10.1038/s41467-020-14464-0

Fitzsimmons, J. N., Bundy, R. M., Al-Subiai, S. N., Barbeau, K. A., & Boyle, E. A. (2015). The composition of dissolved iron in the dusty surface ocean: An exploration using size-fractionated iron-binding ligands. *Marine Chemistry*, *173*, 125–135. https://doi.org/10.1016/j.marchem.2014.09.002

Fourquez, M., Bressac, M., Deppeler, S. L., Ellwood, M., Obernosterer, I., Trull, T. W., & Boyd, P. W. (2020). Microbial Competition in the Subpolar Southern Ocean: An Fe–C Co-limitation Experiment. *Frontiers in Marine Science*, *6*. https://doi.org/10.3389/fmars.2019.00776

Gledhill, M, & van den Berg, C. M. G. (1995). Measurement of the redox speciation of iron in seawater by catalytic cathodic stripping voltammetry. *Marine Chemistry*, *50*(1–4), 51–61.

Gledhill, Martha, & Buck, K. N. (2012). The organic complexation of iron in the marine environment: A review. *Frontiers in Microbiology*, *3*(69). https://doi.org/10.3389/fmicb.2012.00069

Groussman, R. D., Parker, M. S., & Armbrust, E. V. (2015). Diversity and evolutionary history of iron metabolism genes in diatoms. *PLoS ONE*, *10*(6). https://doi.org/10.1371/journal.pone.0129081

Hassler, C. S., Schoemann, V., Boye, M., Tagliabue, A., Rozmarynowycz, M., & McKay, R. M. L. (2012). Iron bioavailability in the Southern Ocean. In R. Gibson, R. Atkinson, J. Gordon, & R. Hughes (Eds.), *Oceanography and Marine Biology: An annual review* (1st ed., Vol. 50, pp. 1–64). https://doi.org/10.1201/b12157

Hassler, C. S., Schoemann, V., Nichols, C. M., Butler, E. C. V., & Boyd, P. W. (2011). Saccharides enhance iron bioavailability to Southern Ocean phytoplankton. *Proceedings of the National Academy of Sciences*. https://doi.org/10.1073/pnas.1010963108

Hatta, M., Measures, C. I., Wu, J., Roshan, S., Fitzsimmons, J. N., Sedwick, P., & Morton, P. (2015). An overview of dissolved Fe and Mn distributions during the 2010-2011 U.S. GEOTRACES north Atlantic cruises: GEOTRACES GA03. *Deep-Sea Research Part II: Topical Studies in Oceanography*. https://doi.org/10.1016/j.dsr2.2014.07.005

Hillebrand, H., Dürselen, C. D., Kirschtel, D., Pollingher, U., & Zohary, T. (1999). Biovolume calculation for pelagic and benthic microalgae. *Journal of Phycology*, *35*(2). https://doi.org/10.1046/j.1529-8817.1999.3520403.x

Hopkinson, B. M., & Barbeau, K. A. (2008). Interactive influences of iron and light limitation on phytoplankton at subsurface chlorophyll maxima in the eastern North Pacific. *Limnology and Oceanography*. https://doi.org/10.4319/lo.2008.53.4.1303

Hudson, R. J. ., & Morel, F. M. M. (1990). lron transport in marine phytoplankton: Kinetics of cellular and medium coordination reactions. *Limnology and Oceanography*, *35*(5), 1002–1020. https://doi.org/10.4319/lo.1990.35.5.1002

Hudson, R. J. ., & Morel, F. M. M. (1993). Trace metal transport by marine microorganisms: implications of metal coordination kinetics. *Deep-Sea Research*, *40*(1), 129–150.

Huntsman, S. A., & Sunda, W. G. (1980a). The role of trace metals in regulating phytoplankton growth. In I. I. M. [ed.] (Ed.), *The Physiological Ecology of Phytoplankton* (Vol. 7, pp. 285–328). Blackwell.

Huntsman, S. A., & Sunda, W. G. (1980b). The role of trace metals in regulating phytoplankton growth with emphasis on Fe, Mn and Cu [iron, manganese, copper]. *Plant Physiology and Biochemistry*, *7*, 315–328.

Hurst, M. P., Aguilar-Islas, A. M., & Bruland, K. W. (2010). Iron in the southeastern Bering Sea: Elevated leachable particulate Fe in shelf bottom waters as an important source for surface waters. *Continental Shelf Research*, *30*(5), 467–480. https://doi.org/10.1016/j.csr.2010.01.001

Johnson, K. S., Gordon, R. M., & Coale, K. H. (1997). What controls dissolved iron concentrations in the world ocean? *Marine Chemistry*, *57*(3–4), 137–161. Retrieved from http://www.sciencedirect.com/science/article/pii/S0304420397000431%5Cnpapers2://publication/uuid/11D941FB-7A6A-4BE6-A827-AFA729AD0523

Kaupp, L. J., Measures, C. I., Selph, K. E., & Mackenzie, F. T. (2011). The distribution of dissolved Fe and Al in the upper waters of the Eastern Equatorial Pacific. *Deep-Sea Research Part II: Topical Studies in Oceanography*. https://doi.org/10.1016/j.dsr2.2010.08.009

King, A. L., Sañudo-Wilhelmy, S. A., Boyd, P. W., Twining, B. S., Wilhelm, S. W., Breene, C., … Hutchins, D. A. (2012). A comparison of biogenic iron quotas during a diatom spring bloom using multiple approaches. *Biogeosciences*, *9*(2), 667–687. https://doi.org/10.5194/bg-9-667-2012

Kustka, A. B., Allen, A. E., & Morel, F. M. M. (2007). Sequence analysis and transcriptional regulation of iron acquisition genes in two marine diatoms. *Journal of Phycology*, *43*(4), 715–729. https://doi.org/10.1111/j.1529-8817.2007.00359.x

Lampe, R. H., Cohen, N. R., Ellis, K. A., Bruland, K. W., Maldonado, M. T., Peterson, T. D., … Marchetti, A. (2018). Divergent gene expression among phytoplankton taxa in response to upwelling. *Environmental Microbiology*. https://doi.org/10.1111/1462-2920.14361

Landry, M. R., Selph, K. E., Taylor, A. G., Décima, M., Balch, W. M., & Bidigare, R. R. (2011). Phytoplankton growth, grazing and production balances in the HNLC equatorial Pacific. *Deep-Sea Research Part II: Topical Studies in Oceanography*, *58*(3–4), 524–535. https://doi.org/10.1016/j.dsr2.2010.08.011

Lis, H., Shaked, Y., Kranzler, C., Keren, N., & Morel, F. (2015a). Iron bioavailability to phytoplankton:

an empirical approach. *The Isme Journal*, *9*, 1003–1013. https://doi.org/10.1038/ismej.2014.199 https://www.nature.com/articles/ismej2014199#supplementary-information

Lis, H., Shaked, Y., Kranzler, C., Keren, N., & Morel, F. M. M. (2015b). Iron bioavailability to phytopalnkton: an emperical approach. *ISME Journal*, *9*, 1003–1013.

Lommer, M., Proebst, S., Allen, A., Maheswari, U., Bowler, C., & LaRoche, J. (2007). The photosynthetic response of a marine diatom to iron limitation. *Photosynthesis Research*, *91*(2–3), 301.

Macrellis, H. M., Trick, C. G., Rue, E. L., Smith, G., & Bruland, K. W. (2001). Collection and detection of natural iron-binding ligands from seawater. *Marine Chemistry*, *76*(3), 175–187. https://doi.org/10.1016/S0304-4203(01)00061-5

Maldonado, M T, Boyd, P. W., Harrison, P. J., & Price, N. M. (1999). Co-limitation of phytoplankton growth by light and Fe during winter in the NE subarctic Pacific Ocean. *Deep-Sea Research II*, *46*, 2475–2485.

Maldonado, M T, & Price, N. M. (2001). Reduction and transport of organically bound iron by Thalassiosira oceanica (Bacillariophyceae). *Journal of Phycology*, *37*, 298–309.

Maldonado, M T, Strzepek, R. F., Sander, S., & Boyd, P. W. (2005). Acquisition of iron bound to strong organic complexes, with different Fe binding groups and photochemical reactivities, by plankton communities in Fe-limited subantarctic waters. *Global Biogeochemical Cycles*, *19*(4). https://doi.org/Gb4s2310.1029/2005gb002481

Maldonado, Maria T., & Price, N. M. (1999). Utilization of iron bound to strong organic ligands by plankton communities in the subarctic Pacific Ocean. *Deep-Sea Research Part II: Topical Studies in Oceanography*. https://doi.org/10.1016/S0967-0645(99)00071-5

Marchetti, A, & Maldonado, M. T. (2016). Iron. In M. A. Borowitzka, J. Beardall, & J. A. Raven (Eds.), *The Physiology of Microalgae* (pp. 233–280). New York: Springer.

Marchetti, Adrian, Schruth, D. M., Durkin, C. A., Parker, M. S., Kodner, R. B., Berthiaume, C. T., … Armbrusta, E. V. (2012). Comparative metatranscriptomics identifies molecular bases for the physiological responses of phytoplankton to varying iron availability. *Proceedings of the National Academy of Sciences of the United States of America*, *109*(6), E317–E325. https://doi.org/10.1073/pnas.1118408109

Mawji, E., Gledhill, M., Milton, J. A., Tarran, G. A., Ussher, S., Thompson, A., … Achterberg, E. P. (2008). Hydroxamate siderophores: Occurrence and importance in the Atlantic Ocean. *Environmental Science and Technology*, *42*(23), 8675–8680. https://doi.org/10.1021/es801884r

Mawji, E., Schlitzer, R., Dodas, E. M., Abadie, C., Abouchami, W., Anderson, R. F., … Zimmer, L. A. (2014, December). The GEOTRACES Intermediate Data Product 2014. *Marine Chemistry*, Vol. 177, pp. 1–8. https://doi.org/10.1016/j.marchem.2015.04.005

McQuaid, J. B., Kustka, A. B., Oborník, M., Horák, A., McCrow, J. P., Karas, B. J., … Allen, A. E. (2018). Carbonate-sensitive phytotransferrin controls high-affinity iron uptake in diatoms. *Nature*, *555*(7697), 534–537. https://doi.org/10.1038/nature25982

Mellett, T., Brown, M. T., Chappell, P. D., Duckham, C., Fitzsimmons, J. N., Till, C. P., … Buck, K. N. (2018). The biogeochemical cycling of iron, copper, nickel, cadmium, manganese, cobalt, lead, and scandium in a California Current experimental study. *Limnology and Oceanography*, *63*, S425–

S447. https://doi.org/10.1002/lno.10751

Menden-Deuer, S., & Lessard, E. J. (2000). Carbon to volume relationships for dinoflagellates, diatoms, and other protist plankton. *Limnology and Oceanography*, *45*(3), 569–579.

Moffett, J. W., & German, C. R. (2018). The U.S.GEOTRACES Eastern Tropical Pacific Transect (GP16). *Marine Chemistry*. https://doi.org/10.1016/j.marchem.2017.12.001

Moore, C. M., Mills, M. M., Arrigo, K. R., Berman-Frank, I., Bopp, L., Boyd, P. W., … Ulloa, O. (2013). Processes and patterns of oceanic nutrient limitation. *Nature Geoscience*, *6*, 701–710. https://doi.org/10.1038/ngeo1765

Morel, F.M.M., Kustka, A. B. B., & Shaked, Y. (2008). The role of unchelated Fe in the iron nutrition of phytoplankton. *Limnology and Oceanography*, *53*(1), 400–404. https://doi.org/10.4319/lo.2008.53.1.0400

Morel, Francois M.M. (2008). The co-evolution of phytoplankton and trace element cycles in the oceans. *Geobiology*, *6*(3), 318–324. https://doi.org/10.1111/j.1472-4669.2008.00144.x

Morrissey, J., & Bowler, C. (2012). Iron utilization in marine cyanobacteria and eukaryotic algae. *Frontiers in Microbiology*, *3*(43). https://doi.org/10.3389/fmicb.2012.00043

Rafter, P. A., Sigman, D. M., & Mackey, K. R. M. (2017). Recycled iron fuels new production in the eastern equatorial Pacific Ocean. *Nature Communications*, *8*(1100). https://doi.org/10.1038/s41467-017-01219-7

Rue, E. L., & Bruland, K. W. (1995). Complexation of iron(III) by natural organic ligands in the central North Pacific as determined by a new competitive ligand equilibration/ adsorptive cathodic stripping voltammetric method. *Marine Chemistry*, *50*(1–4), 117–138.

Saito, M. A., Goepfert, T. J., & Ritt, J. T. (2008). Some thoughts on the concept of colimitation: Three definitions and the importance of bioavailability. *Limnology and Oceanography*. https://doi.org/10.4319/lo.2008.53.1.0276

Schlitzer, R., Anderson, R. F., Dodas, E. M., Lohan, M., Geibert, W., Tagliabue, A., … Zurbrick, C. (2018). The GEOTRACES Intermediate Data Product 2017. *Chemical Geology*, *493*, 210–223. https://doi.org/10.1016/j.chemgeo.2018.05.040

Sedwick, P. N., Sohst, B. M., Ussher, S. J., & Bowie, A. R. (2015). A zonal picture of the water column distribution of dissolved iron(II) during the U.S. GEOTRACES North Atlantic transect cruise (GEOTRACES GA03). *Deep-Sea Research Part II: Topical Studies in Oceanography*. https://doi.org/10.1016/j.dsr2.2014.11.004

Selph, K. E., Landry, M. R., Taylor, A. G., Yang, E. J., Measures, C. I., Yang, J., … Bidigare, R. R. (2011). Spatially-resolved taxon-specific phytoplankton production and grazing dynamics in relation to iron distributions in the Equatorial Pacific between 110 and 140°W. *Deep-Sea Research Part II: Topical Studies in Oceanography*, *58*(3–4), 358–377. https://doi.org/10.1016/j.dsr2.2010.08.014

Shaked, Y., & Lis, H. (2012). Disassembling iron availability to phytoplankton. *Frontiers in Microbiology*, *3*(123). https://doi.org/10.3389/fmicb.2012.00123

Shaked, Y, Kustka, A. B., & Morel, F. M. M. (2005). A general kinetic model for iron acquisition by eukaryotic phytoplankton. *Limnology and Oceanography*, *50*(3), 872–882. https://doi.org/10.4319/lo.2005.50.3.0872

Shaked, Yeala. (2008). Iron redox dynamics in the surface waters of the Gulf of Aqaba, Red Sea. *Geochimica et Cosmochimica Acta*, *72*(6), 1540–1554. https://doi.org/10.1016/j.gca.2008.01.005

Shaked, Yeala, Buck, K. N., Mellett, T., & Maldonado, M. T. (2020). Insights into the bioavailability of oceanic dissolved Fe from phytoplankton uptake kinetics. *ISME Journal*, *14*(5), 1182–1193. https://doi.org/10.1038/s41396-020-0597-3

Sigman, D. M., & Hain, M. P. (2012). The Biological Productivity of the Ocean | Learn Science at Scitable. *Nature Education Knowledge*.

Stock, C. A., Dunne, J. P., & John, J. G. (2014). Global-scale carbon and energy flows through the marine planktonic food web: An analysis with a coupled physical-biological model. *Progress in Oceanography*, *120*, 1–28. https://doi.org/10.1016/j.pocean.2013.07.001

Strzepek, R F, Maldonado, M. T., Higgins, J. L., Hall, J., Safi, K., Wilhelm, S. W., & Boyd, P. W. (2005). Spinning the "Ferrous Wheel": The importance of the microbial community in an iron budget during the FeCycle experiment. *Global Biogeochemical Cycles*, *19*(4). https://doi.org/Gb4s2610.1029/2005gb002490

Strzepek, Robert F., Maldonado, M. T., Hunter, K. A., Frew, R. D., & Boyd, P. W. (2011). Adaptive strategies by Southern Ocean phytoplankton to lessen iron limitation: Uptake of organically complexed iron and reduced cellular iron requirements. *Limnology and Oceanography*, *56*(6), 1983–2002. https://doi.org/10.4319/lo.2011.56.6.1983

Sunda, W. G., & Huntaman, S. A. (1997). Interrelated influence of iron, light and cell size on marine phytoplankton growth. *Nature*, *390*(6658), 389–392. https://doi.org/10.1038/37093

Sunda, William G., & Huntsman, S. A. (1995). Iron uptake and growth limitation in oceanic and coastal phytoplankton. *Marine Chemistry*, *50*(1–4), 189–206. https://doi.org/10.1016/0304-4203(95)00035-P

Sunda, William G., Price, N. M., & Morel, F. M. M. (2005). Trace Metal Ion Buffers and Their Use in Culture Studies. In *Algal Culturing Techniques*. https://doi.org/10.1016/b978-012088426-1/50005-6

Sutak, R., Camadro, J. M., & Lesuisse, E. (2020). Iron Uptake Mechanisms in Marine Phytoplankton. *Frontiers in Microbiology*, Vol. 11. https://doi.org/10.3389/fmicb.2020.566691

Tagliabue, A, Barrier, N., Du Pontavice, H., Kwiatkowski, L., Aumont, O., Bopp, L., … Maury, O. (2020). An iron cycle cascade governs the response of equatorial Pacific ecosystems to climate change. *Global Change Biology*, *26*, 6168–6179.

Tagliabue, Alessandro, Aumont, O., Death, R., Dunne, J. P., Dutkiewicz, S., Galbraith, E., … Yool, A. (2016). How well do global ocean biogeochemistry models simulate dissolved iron distributions? *Global Biogeochemical Cycles*, *30*(2), 149–174. https://doi.org/10.1002/2015GB005289

Tagliabue, Alessandro, Bowie, A. R., Boyd, P. W., Buck, K. N., Johnson, K. S., & Saito, M. A. (2017). The integral role of iron in ocean biogeochemistry. *Nature*, *543*(7643), 51–59. https://doi.org/10.1038/nature21058

Tagliabue, Alessandro, Bowie, A. R., DeVries, T., Ellwood, M. J., Landing, W. M., Milne, A., … Boyd, P. W. (2019). The interplay between regeneration and scavenging fluxes drives ocean iron cycling. *Nature Communications*, *10*(1). https://doi.org/10.1038/s41467-019-12775-5

Tanioka, T., Fichot, C. G., & Matsumoto, K. (2020). Toward Determining the Spatio-Temporal

Variability of Upper-Ocean Ecosystem Stoichiometry From Satellite Remote Sensing. *Frontiers in Marine Science*, *7*(604893). https://doi.org/10.3389/fmars.2020.604893

Till, C. P., Solomon, J. R., Cohen, N. R., Lampe, R. H., Marchetti, A., Coale, T. H., & Bruland, K. W. (2019). The iron limitation mosaic in the California Current System: Factors governing Fe availability in the shelf/near-shelf region. *Limnology and Oceanography*. https://doi.org/10.1002/lno.11022

Timmermans, K. R., Gerringa, L. J. A., de Baar, H. J. W., van der Wagt, B., Veldhuis, M. J. W., de Jong, J. T. M., … Boye, M. (2001). Growth rates of large and small Southern Ocean diatoms in relation to availability of iron in natural seawater. *Limnology and Oceanography*, *46*(2), 260–266.

Twining, B. S., Baines, S. B., Fisher, N. S., Maser, J., Vogt, S., Jacobsen, C., … Sañudo-Wilhelmy, S. A. (2003). Quantifying trace elements in individual aquatic protist cells with a synchrotron X-ray fluorescence microprobe. *Analytical Chemistry*, *75*(15), 3806. Retrieved from http://www.scopus.com/inward/record.url?eid=2-s2.0-0042062394&partnerID=40&md5=cc2f933ade46a4ff461369e284d4de14

Twining, B. S., Rauschenberg, S., Baer, S. E., Lomas, M. W., Martiny, A. C., & Antipova, O. (2019). A nutrient limitation mosaic in the eastern tropical Indian Ocean. *Deep-Sea Research Part II: Topical Studies in Oceanography*, *166*, 125–140. https://doi.org/10.1016/j.dsr2.2019.05.001

Twining, Benjamin S., Antipova, O., Chappell, P. D., Cohen, N. R., Jacquot, J. E., Mann, E. L., … Tagliabue, A. (2021). Taxonomic and nutrient controls on phytoplankton iron quotas in the ocean. *Limnology and Oceanography Letters*, *6*(2), 96–106. https://doi.org/https://doi.org/10.1002/lol2.10179

Twining, Benjamin S., & Baines, S. B. (2013). The Trace Metal Composition of Marine Phytoplankton. *Annual Review of Marine Science*, *5*, 191–215. https://doi.org/10.1146/annurev-marine-121211-172322

Twining, Benjamin S., Baines, S. B., Bozard, J. B., Vogt, S., Walker, E. A., & Nelson, D. M. (2011). Metal quotas of plankton in the equatorial Pacific Ocean. *Deep-Sea Research Part II: Topical Studies in Oceanography*. https://doi.org/10.1016/j.dsr2.2010.08.018

Twining, Benjamin S., Baines, S. B., & Fisher, N. S. (2004). Element stoichiometries of individual plankton cells collected during the Southern Ocean Iron Experiment (SOFeX). *Limnology and Oceanography*. https://doi.org/10.4319/lo.2004.49.6.2115

Twining, Benjamin S., Baines, S. B., Fisher, N. S., & Landry, M. R. (2004). Cellular iron contents of plankton during the Southern Ocean Iron Experiment (SOFeX). *Deep-Sea Research Part I: Oceanographic Research Papers*. https://doi.org/10.1016/j.dsr.2004.08.007

Twining, Benjamin S., Rauschenberg, S., Morton, P. L., Ohnemus, D. C., & Lam, P. J. (2015). Comparison of particulate trace element concentrations in the North Atlantic Ocean as determined with discrete bottle sampling and in situ pumping. *Deep-Sea Research Part II: Topical Studies in Oceanography*. https://doi.org/10.1016/j.dsr2.2014.11.005

Twining, Benjamin S., Rauschenberg, S., Morton, P. L., & Vogt, S. (2015). Metal contents of phytoplankton and labile particulate material in the North Atlantic Ocean. *Progress in Oceanography*. https://doi.org/10.1016/j.pocean.2015.07.001

Waite, T. D. (2001). Thermodynamics of the Iron System in Seawater. In D. R. Turner & K. A. Hunter (Eds.), *The Biogeochemistry of Iron in Seawater* (pp. 291–342). New York: John Wiley & Sons.

Wilhelm, S. W., King, A. L., Twining, B. S., LeCleir, G. R., DeBruyn, J. M., Strzepek, R. F., … Hutchins, D. A. (2013). Elemental quotas and physiology of a southwestern pacific ocean plankton community as a function of iron availability. *Aquatic Microbial Ecology*, *68*(3), 185–194. https://doi.org/10.3354/ame01611

Worms, I., Simon, D. F., Hassler, C. S., & Wilkinson, K. J. (2006). Bioavailability of trace metals to aquatic microorganisms: importance of chemical, biological and physical processes on biouptake. *Biochimie*, *88*(11), 1721–1731. https://doi.org/10.1016/j.biochi.2006.09.008